Available online at www.sciencedirect.com
ScienceDirect
Icarus 192 (2007) 588–604
ICARUS
www.elsevier.com/locate/icarus

Particle stirring in turbulent gas disks: Including orbital oscillations

Andrew N. Youdin *, Yoram Lithwick

C.I.T.A., University of Toronto, 60 St. George St., Toronto, ON M5S 3H8, Canada

Received 21 March 2007; revised 26 June 2007

Available online 5 September 2007

Abstract

We describe the diffusion and random velocities of solid particles due to stochastic forcing by turbulent gas. We include the orbital dynamics of Keplerian disks, both in-plane epicycles and vertical oscillations. We obtain a new result for the diffusion of solids. The Schmidt number (ratio of gas to particle diffusivity) is $Sc \approx 1 + (\Omega t_{\rm stop})^2$, in terms of the particle stopping time $t_{\rm stop}$ and the orbital frequency Ω. The standard result, $Sc = 1 + t_{\rm stop}/t_{\rm eddy}$, in terms of the eddy turnover time, $t_{\rm eddy}$, is shown to be incorrect. The main difference is that Sc rises quadratically, not linearly, with stopping time. Consequently, particles larger than $\sim$10 cm in protoplanetary disks will suffer less radial diffusion and will settle closer to the midplane. Such a layer of boulders would be more prone to gravitational collapse. Our predictions of RMS speeds, vertical scale height and diffusion coefficients will help interpret numerical simulations. We confirm previous results for the vertical stirring of particles (scale heights and random velocities), and add a correction for arbitrary ratios of eddy to orbital times. The particle layer becomes thinner for $t_{\rm eddy} > 1/\Omega$ with the strength of turbulent diffusion held fixed. We use two analytic techniques—the Hinze–Tchen formalism and the Fokker–Planck equation with velocity diffusion—with identical results when the regimes of validity overlap. We include simple physical arguments for the scaling of our results.

Keywords: Disks; Planetary formation; Solar nebula

1. Introduction

The stirring of particles by turbulent gas is a fundamental problem in fluid dynamics. It is especially important in studying the formation of planetesimals because the (non-Keplerian) motion of particles below about a kilometer in radius is strongly influenced by gas drag. Our goal here is to include, for the first time, the effect of Keplerian orbital dynamics on the random speeds and diffusion of particles.

Circumstellar disks are thought to be turbulent. Turbulence drives accretion onto protostars by dissipating Keplerian shear and transferring angular momentum radially outwards. The magnetorotational instability (Balbus and Hawley, 1991) is a leading candidate for the source of disk turbulence despite concerns that protoplanetary disks may be insufficiently ionized in "dead zones" near the disk midplane (Gammie, 1996; Semenov et al., 2004). Convection (Lin and Papaloizou, 1980; Klahr et al., 1999) and purely hydrodynamical mechanisms (Dubrulle et al., 2005; Rincon et al., 2007; Lithwick, 2007) to generate turbulence are being actively investigated. For this work, we remain agnostic as to the source of disk turbulence, as well as to its detailed properties.

While turbulence is beneficial for accretion onto stars, it is thought to hinder the growth of planetesimals in disks. The gravitational collapse of smaller solids into planetesimals (Safronov, 1969; Goldreich and Ward, 1973; Youdin and Shu, 2002) is opposed by turbulence (Weidenschilling, 1980). Turbulent diffusion balances the vertical settling of dust grains and larger solids to the midplane (Cuzzi et al., 1993; Sekiya, 1998; Dubrulle et al., 1995; Carballido et al., 2006), thereby setting the midplane volume density for a given surface density. The velocity dispersion of solids determines the Toomre (1964) gravitational stability, or Q, parameter for thin disks. By analogy with single component disks, it is argued that gravitational collapse requires densities above a critical threshold, and/or Q values below unity. This overlooks the important role of gas drag in the collapse of solids, which removes such thresholds

* Corresponding author.
E-mail address: youd@cita.utoronto.ca (A.N. Youdin).

0019-1035/$ – see front matter
doi:10.1016/j.icarus.2007.07.012

(Ward, 1976, 2000; Youdin, 2005a, 2005b). These works show that collapse into rings over many dynamical times is possible even for nominally gravitationally stable values of midplane density and velocity dispersion. Radial diffusion plays an important role in this type of dissipative collapse. This work establishes formulae for vertical density structure, velocity dispersion and radial diffusion of particles in turbulent gas disks. These results can be used to construct more realistic models of gravitational collapse of solids into planetesimals.

Turbulent stirring also determines the relative speeds with which particles collide (Völk et al., 1980) and can be used to help determine when particles coagulate, fragment, or inelastically dissipate energy (Dominik and Tielens, 1997). Since our work does not include the spatial dynamics internal to eddies we do not specifically address relative velocities. However for large solids with long aerodynamic stopping times the relative speeds are just the RMS random speeds (added in quadrature). Other works give refinements (Markiewicz et al., 1991) and analytical fits (Ormel and Cuzzi, 2007) to the Völk et al. (1980) relative velocities, and investigate the implications for coagulation, given various assumptions about particle sticking (Mizuno et al., 1988). Völk et al. (1980) does not give results for particle diffusion and does not include orbital dynamics.

Recent years have seen a remarkable advance in numerical simulations of the dynamics of solid particles in turbulent gas disks (e.g., Johansen and Klahr, 2005; Fromang and Nelson, 2005; Carballido et al., 2005). The results of this work can be used to make detailed comparisons to the motion of test particles in these simulations. Simulations have now begun to include the dynamical feedback of particles on gas dynamics (Johansen et al., 2006a; Johansen and Youdin, 2007). These works find that streaming instabilities (Youdin and Goodman, 2005; Youdin and Johansen, 2007) lead to the clumping of particles, an effect our turbulent stirring models do not include. Other particle concentration mechanisms, including long-lived vortices (de la Fuente Marcos and Barge, 2001), turbulent pressure enhancements (Johansen et al., 2006b), or low-enstrophy regions at the dissipation scale (Hogan and Cuzzi, 2007) are neglected as well.

The standard result for particle diffusion was given by Cuzzi et al. (1993) (see Section 4.1.1). We improve on this result in two ways. First we evaluate the statistical growth of particle separations, instead of making the (incorrect) assumption that diffusion is proportional to kinetic energy. Second, we include orbital dynamics, both vertical oscillations and the epicyclic motion that couples radial and azimuthal forcing. Since the Cuzzi et al.'s (1993) result was correct for small, tightly-coupled solids, many previous results are unaffected by the error.

This work is organized as follows. We introduce the relevant timescales of the problem in Section 2. Our main results are justified with simple order of magnitude estimates in Section 3. We review particle stirring with the Hinze–Tchen formalism in Section 4.1, before extending it to include vertical oscillations in Section 4.2 and epicyclic oscillations in Section 4.3. We confirm our results with the Fokker–Planck equation in Section 5. Section 6 addresses neglected effects such as collisions (Section 6.1), the "crossing trajectories" effect (Section 6.2), and particle feedback on gas dynamics (Section 6.3). We discuss the implications of our results in Section 7.

2. Timescales and dimensionless parameters

Particle stirring in turbulent gas disks is characterized by three timescales: $t_{\rm stop}$, $t_{\rm eddy}$, and $1/\Omega$. The particle stopping time, $t_{\rm stop}$, is the exponential timescale for the decay of relative motion with gas via drag forces, e.g., Eq. (7), and $t_{\rm stop}$ is an increasing function of particle size (for a given material density) as detailed in Appendix A. The eddy time, $t_{\rm eddy}$, is the correlation time of turbulent fluctuations (defined formally in Eq. (11)). For Kolmogorov turbulence, $t_{\rm eddy}$ is also the turnover time of the largest-scale eddies. Smaller eddies have shorter turnover times, and contribute less to the turbulent kinetic energy. The orbital frequency, Ω, is also the vertical and epicyclic oscillation frequency in Keplerian disks, where $1/\Omega$ is also the radial shear time (modulo 3/2). For reference, Table 2 collects most of the symbols used in this work.

We define three dimensionless parameters, of which two are independent,

$$\tau_{\rm s} \equiv \Omega t_{\rm stop}, \tag{1a}$$

$$\tau_{\rm e} \equiv \Omega t_{\rm eddy}, \tag{1b}$$

$$St \equiv t_{\rm stop}/t_{\rm eddy} = \tau_{\rm s}/\tau_{\rm e}, \tag{1c}$$

to describe the parameter space of turbulent stirring, as shown schematically in Fig. 1. The dimensionless stopping time measures whether particles are tightly ($\tau_{\rm s} \ll 1$) or weakly ($\tau_{\rm s} \gg 1$) coupled to unperturbed circular gas orbits. The Stokes number, St, also measures particle coupling, but to turbulent fluctuations. The dimensionless eddy time, $\tau_{\rm e}$, describes the effect of orbital shear on eddies. If eddies are destroyed in a shear time, then $\tau_{\rm e} \sim 1$, and some local MRI simulations support this choice (Fromang and Papaloizou, 2006).[1] Orbital dynamics plays no role in turbulence with $\tau_{\rm e} \ll 1$, which is unsheared and would require an energy source other than orbital differential rotation, perhaps convection. Turbulent eddies with $\tau_{\rm e} \gg 1$[2] are extended azimuthally by orbital shear. MRI turbulence might well give rise to $\tau_{\rm e} \gg 1$ eddies as indicated by the extended azimuthal structure seen in MRI simulations (Hawley et al., 1995) and perhaps particle trapping seen in global MRI simulations (Fromang and Nelson, 2005).

Given our ignorance of the detailed properties of turbulence in protoplanetary disks, we consider deviations from the favored value of $\tau_{\rm e} = 1$ (in which case $\tau_{\rm s} = St$). By keeping $\tau_{\rm e}$

[1] Note however that Fromang and Papaloizou (2006) use a local Eulerian measure of the eddy time, which they argue should be similar to the more appropriate Lagrangian measure.

[2] Even though long-lived vortices are often invoked to trap particles, turbulence with $\tau_{\rm e} \gg 1$ does not necessarily concentrate particles within eddies. To trap particles, a vortex must live for many circulation times (the time for fluid to circulate within a vortex). For example, in Appendix B we introduce a simple model for $\tau_{\rm e} \gg 1$ turbulence that is composed of vortices that live for a single circulation time. Even though their circulation time is much longer than the orbital time, these vortices cannot concentrate particles in their lifetime.

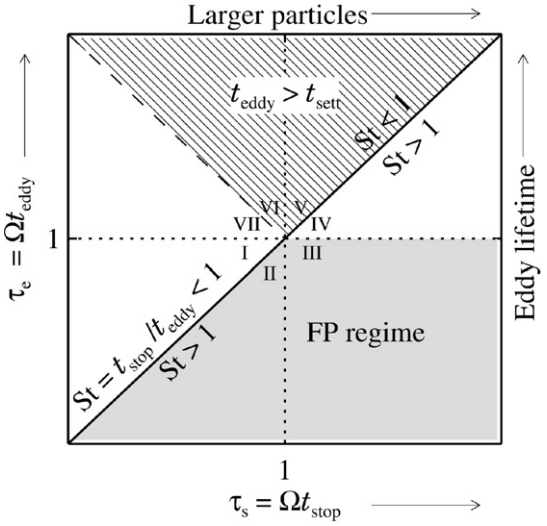

Fig. 1. Schematic plot of the parameter space for particle stirring with eddy time vs particle stopping time, both normalized to the orbital frequency. Dotted lines indicate where these τ_e and τ_s parameters are unity. The straight line of slope one demarcates Stokes number of unity, where particles are marginally coupled to eddies. The shaded region indicates where a Fokker–Planck approach is valid because the stochastic forcing time, t_{eddy}, is short. In the upper hatched region, t_{eddy} exceeds the vertical settling time. Roman numerals label regions where timescales are ordered as indicated in Table 1.

general, we also gain a physical understanding of its effect. Appendix B describes a simple model for turbulent velocities with arbitrary τ_e, which includes basic dynamical considerations of shearing disks and is useful in making numerical evaluations. We include general expressions for our results so other realizations of turbulence can be considered.

Previous works on particle stirring which neglect orbital dynamics effectively assume $\tau_s, \tau_e \ll 1$ (regions I and II in the lower left corner of Fig. 1). Our study of vertical motions in Section 4.2, and epicyclic oscillations in Section 4.3 includes all regions of Fig. 1. The shaded region in Fig. 1 indicates where t_{eddy} is the shortest timescale in the problem (regions II and III). Here the Fokker–Planck equation can model turbulent stirring with the inclusion of velocity diffusion, as done here (Section 5) for in-plane motion and by Carballido et al. (2006) for the vertical settling problem.

The vertical settling timescale, t_{sett}, of tightly coupled particles, $\tau_s \ll 1$, at the terminal velocity for stellar gravity is $t_{sett} = 1/(\Omega\tau_s)$. The vertical oscillations of loosely coupled particles damp in $t_{sett} = t_{stop}$. These results can be combined to give:

$$\Omega t_{sett} \simeq \tau_s + 1/\tau_s. \tag{2}$$

The hatched triangle in Fig. 1 (regions V and VI) shows where the eddy times exceed particle settling times.

2.1. Aside on the Schmidt number

This paper obtains a new result for the spatial diffusion of heavy particles, D_p. We compare this to the spatial diffusion of gaseous contaminants, D_g, which depends only on the time-integrated correlation of turbulent velocities (Eqs. (11a)–(11c)). Following Cuzzi et al. (1993) we call the ratio $Sc \equiv D_g/D_p$, the Schmidt number, and we generally expect $Sc \gtrsim 1$ because particles should not diffuse faster than the gas. This notation is somewhat unfortunate as it differs from the standard fluid dynamical convention. In fluid dynamics $Sc_{hydro} \equiv \nu/D_g$, is the ratio of the viscous (momentum) diffusion to mass diffusion (of the fluid itself for the typical single fluid case). This ratio is astrophysically important since it determines the diffusion of gas (or small particle) contaminants relative to the accretion flow (Stevenson, 1990; Turner et al., 2006). Most numerical studies of particle diffusion (Johansen and Klahr, 2005; Carballido et al., 2005) measure the Schmidt number for particles as the ratio $Sc_{sim} = \nu/D_p$, where ν includes the total accretion stress, with Reynolds and Maxwell stress contributions, since the turbulence is MRI-driven. Thus Sc_{sim} combines the effects of particle dynamics and angular momentum transport. Indeed, Johansen et al. (2006c) found that imposed vertical magnetic flux significantly affected Sc_{sim}. This explains why there have been reports of Sc_{sim} both above and below unity for tightly coupled particles, while we find [with Cuzzi et al. (1993)] that $Sc = 1$ in this limit. To isolate the effects of particle dynamics, and to compare directly with Cuzzi et al. (1993), we opt for the Cuzzi et al. (1993) convention of Sc. Comparison of our results with numerical simulations requires measurement of both the diffusion of heavy particles, D_p, and Lagrangian tracers of the fluid motion, D_g.

3. Physical scaling arguments

Our main results can be understood with simple physical arguments in limiting cases. We assume isotropic turbulence with a RMS speed of δV_g. The turbulent diffusion coefficient for gas is $D_g \sim \delta V_g^2 t_{eddy}$.

3.1. No orbital oscillations: $\tau_s \ll 1, \tau_e \ll 1$

We first ignore orbital effects by taking $\tau_e \ll 1$ and $\tau_s \ll 1$ (lower left quadrant of Fig. 1), so the particle response depends only on St. For $St \ll 1$ particles are well coupled to eddies. Thus the particle RMS velocities, $\delta V_p \sim \delta V_g$, and diffusion coefficient, $D_p \sim D_g$, are the same as for the turbulent gas.

For $St \gg 1$ turbulent eddies wash over loosely coupled particles, and the kicks give a random walk in velocity. Each kick of duration t_{eddy} has an amplitude $V_{kick} \sim \delta V_g t_{eddy}/t_{stop}$ in a random direction. Particle motions equilibrate with the turbulent forcing in t_{stop}. Thus after $N = t_{stop}/t_{eddy}$ kicks, the random velocity will saturate at:

$$\delta V_p \approx \sqrt{N} V_{kick} = \delta V_g/\sqrt{St} \quad \text{for } St \gg 1. \tag{3}$$

By combining the large and small St limits we recover the standard result of Eq. (13).

To estimate particle diffusion for $St \gg 1$, note it takes t_{stop} to deviate the particle velocity by order unity. Thus the particle mean free path is $\ell_p = \delta V_p t_{stop}$, and the diffusion is $D_p \sim \delta V_p \ell_p \sim \delta V_p^2 t_{stop} \sim \delta V_g^2 t_{eddy} \sim D_g$. With increasing St, the longer mean free path cancels the lower velocities to maintain $D_p = D_g$ for all St in agreement with Eq. (14), which also

ignores orbital oscillations. Analysis of previous results which erroneously claim that D_p decreases for large St in this regime can be found in Section 4.1.1.

3.2. Including orbital oscillations: $\tau_s \gg 1 \gg \tau_e$

To better understand orbital oscillations we consider $\tau_s \gg 1$, so that particles decouple from gas orbits, but keep $\tau_e \ll 1$. Thus particles receive many small kicks during a vertical oscillation or an epicycle and $St \gg 1$. This region occupies the lower right quadrant of Fig. 1. The particle velocity response is still a random walk, which saturates at $\delta V_p \sim \delta V_g/\sqrt{St}$ as above, unaffected by oscillations with frequency Ω. This is confirmed in Eqs. (20) and (35a)–(35c), where the latter includes corrections for the ratio of radial to azimuthal epicyclic motion.

Spatial particle diffusion is interrupted by epicyclic oscillations with a length scale $\ell_{epi} \sim \delta V_p/\Omega$. Vertical oscillations are centered on the midplane, and thus do not freely diffuse over long times. For epicyclic motion, we estimate diffusion by noting that the guiding center shifts by ℓ_{epi} every t_{stop}, because the velocity changes by δV_p in this same interval. This gives a diffusion coefficient:

$$D_p \sim \frac{\ell_{epi}^2}{t_{stop}} \sim \frac{\delta V_p^2}{\Omega \tau_s} \sim \frac{\delta V_g^2 t_{eddy}}{\tau_s^2} \sim \frac{D_g}{\tau_s^2}. \tag{4}$$

This can be confirmed by considering the more incremental changes during each orbital oscillation. Every $1/\Omega$ a particle receives $N_{epi} = 1/\tau_e$ velocity kicks of $V_{kick} \sim \delta V_g/St$ to give a velocity change, $\delta V_{epi} \sim V_{kick}\sqrt{N_{epi}} \sim \delta V_g \sqrt{\tau_e}/\tau_s$, every orbital period. Thus every orbital period gives a shift in the guiding center position of $\delta \ell_{epi} \sim \delta V_{epi}/\Omega$. A random walk with steps of size $\delta \ell_{epi}$ every orbital time gives a particle diffusion coefficient $D_p \sim \delta \ell_{epi}^2 \Omega \sim D_g/\tau_s^2$ as in Eq. (4).

If we include the $\tau_s \ll 1$ limit where orbital effects are negligible, then our estimate of the Schmidt number is

$$Sc \equiv \frac{D_g}{D_p} \sim 1 + \tau_s^2. \tag{5}$$

To order unity, this agrees with the precise result for radial diffusion, Eq. (37), which holds for all τ_e. Thus orbital oscillations reduce the diffusion of loosely coupled particles.

3.3. Vertical scale height

We obtain the particle scale height, H_p, by equating the diffusion time, H_p^2/D_p, and the settling time (Eqs. (2) and (5)). The result,

$$H_p \sim \sqrt{\frac{D_g}{\Omega \tau_s}}, \tag{6}$$

holds for arbitrary τ_s and agrees with our detailed results in Eq. (21) and previous works. In the loose coupling limit, H_p can be obtained simply by noting that $H_p \sim \delta V_p/\Omega$ for vertical oscillations. Carballido et al. (2006) computed H_p in the loose coupling limit both analytically and with hydrodynamic simulations and found Eq. (6).[3] The simple link between Eqs. (5) and (6) confirms that orbital oscillations weaken particle diffusion.

4. Fourier solution of Langevin equations

4.1. Hinze–Tchen formalism: No orbital oscillations

We summarize the classic derivation of Hinze (1959) and Tchen (1947) for turbulent transport of particles in the absence of orbital effects or other external forces (reviewed in Fan and Zhu, 1998). A Langevin equation describes the forcing of particle velocities, u_p, by a gas velocity, u_g, with stochastic fluctuations as

$$\frac{du_p}{dt} = -\frac{u_p}{t_{stop}} + \frac{u_g(t)}{t_{stop}}. \tag{7}$$

We restrict our attention to a single dimension with no loss of generality since the motions in different dimensions are uncoupled. The drag force is linear in the relative velocity, which applies in either the Epstein or Stokes regimes. For protoplanetary disks, this requires particle sizes below a_{turb} in Eq. (A.4). Spatial variations in the gas forcing are ignored, because the time to cross an eddy is longer than the eddy lifetime (see Section 6.2).

We decompose u_p and u_g into Fourier modes that vary as $\exp(-\imath\omega t)$. The Fourier amplitudes evolve by Eq. (7) as

$$\hat{u}_p = \frac{\hat{u}_g}{1 - \imath\omega t_{stop}}. \tag{8}$$

The power spectrum of turbulent forcing,

$$\hat{E}_g(\omega) \equiv \langle u_g^2 \rangle \hat{P}(\omega) = \frac{\langle u_g^2 \rangle}{\pi} \frac{t_{eddy}}{1 + \omega^2 t_{eddy}^2}, \tag{9}$$

is normalized to the expectation value of turbulent velocity squared,

$$\langle u_g^2 \rangle = \int_{-\infty}^{\infty} d\omega\, \hat{E}_g. \tag{10}$$

The frequency dependence in Eq. (9) corresponds to exponential decay of time correlations, as the Fourier transform shows, $P(t) = \exp(-|t|/t_{eddy})/(2\pi)$. This spectrum is Kolmogorov since $\hat{P}(\omega) \propto \omega^{-2}$ for frequencies above $1/t_{eddy}$, the integral scale. This equates to the familiar spatial spectra of $\hat{P}(k) \propto k^{-5/3}$ since $k v_k^3 =$ constant, and $v_k = \omega/k$ readily gives $k^{-5/3}\, dk \propto \omega^{-2}\, d\omega$.

Diffusion of tracer particles (i.e., gas) with position, $x_g(t) = \int_0^t u_g(\tau)\, d\tau + x_g(0)$, is given by the statistically averaged

[3] Carballido et al. (2006) also show that both the spatial and velocity distributions are Gaussian with the stated RMS centered on zero velocity at the midplane.

growth rate of squared displacements over long times as

$$D_g \equiv \frac{1}{2}\frac{d\langle x_g^2\rangle}{dt} = \int_0^\infty \langle u_g(\tau)u_g(0)\rangle\, d\tau, \tag{11a}$$

$$= \int_0^\infty d\tau \int_{-\infty}^\infty d\omega\, \hat{E}_g(\omega)e^{(-\imath\omega\tau)}, \tag{11b}$$

$$= \pi \hat{E}_g(0) = \langle u_g^2\rangle t_{eddy}, \tag{11c}$$

where Eq. (11b) equates the velocity autocorrelation function to the Fourier transform of the power spectrum, and Eq. (11c) exploits that the power spectrum is even in ω (equivalent to the time invariance of the correlation function). The final result is the expected product of RMS velocity $\delta V_g = \langle u_g^2\rangle^{1/2}$ and eddy length, $\ell_{eddy} = \delta V_g t_{eddy}$.

The power spectrum of particle motions

$$\hat{E}_p(\omega) = \hat{E}_g(\omega)\frac{|\hat{u}_p|^2}{|\hat{u}_g|^2} = \frac{\hat{E}_g(\omega)}{1+(\omega t_{stop})^2} \tag{12}$$

readily produces the mean squared particle velocities

$$\langle u_p^2\rangle = \int_{-\infty}^\infty d\omega\, \hat{E}_p(\omega) = \frac{\langle u_g^2\rangle t_{eddy}}{t_{eddy}+t_{stop}} = \frac{\langle u_g^2\rangle}{1+St}. \tag{13}$$

This agrees with our physical estimate in Eq. (3), and more importantly, with a detailed treatment that includes the spatial spectrum of eddies (Völk et al., 1980).

Spatial particle diffusion is computed as in Eqs. (11a)–(11c). Since the power spectrum in Eqs. (9) and (12) is also even in ω, we simply have

$$D_p = \pi \hat{E}_p(0) = \langle u_g^2\rangle t_{eddy} = D_g, \tag{14}$$

independent of stopping time. The Schmidt number is $Sc \equiv D_g/D_p = 1$ in this regime, as explained in Section 3 by the longer mean free path for larger t_{stop}.

4.1.1. Comparison with Cuzzi et al. (1993)

The most often cited result for the Schmidt number in the astrophysical literature is from Cuzzi et al. (1993). Their analysis begins exactly as above (Section 4.1): using the Hinze–Tchen formalism with the same temporal power spectrum and ignoring orbital dynamics (see their Appendix B). Instead of calculating diffusion from velocity correlations as in Eqs. (11) and (14), they assume that diffusion coefficients are proportional to the ratio of fluctuating kinetic energies. This gives[4]

$$Sc_{\text{Cuzzi et al. (1993)}} = \langle u_g^2\rangle/\langle u_p^2\rangle = 1+St, \tag{15}$$

which is incorrect since it ignores the role of the particle mean free path. There is no disagreement for low Stokes numbers where $Sc \simeq 1$.

[4] Cuzzi et al. (1993) further add a correction for the "crossing trajectories effect" of particles drifting through eddies with a speed ΔV to get their final result of: $Sc'_{\text{Cuzzi et al. (1993)}} = (1+St)(1+\Delta V^2/\langle u_g^2\rangle)^{1/2}$. This further increases Sc and does not explain the discrepancy. See Section 6.2 for further discussion.

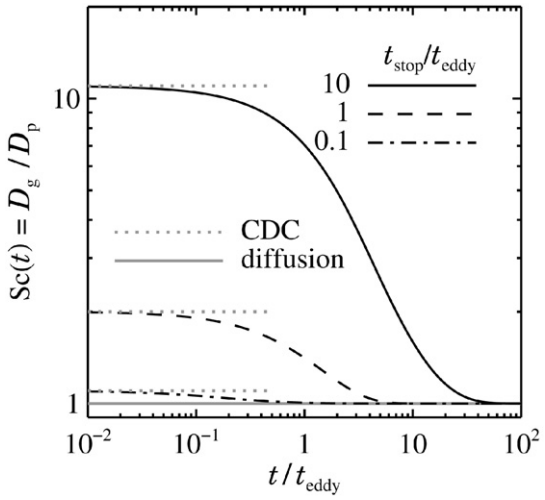

Fig. 2. Schmidt number, the ratio of gas to particle mass transport coefficients, versus time *in the absence of orbital dynamics* or other external forces. Different black curves choose different values of $St = t_{stop}/t_{eddy}$. In the diffusion limit of long times, $Sc = 1$ for all St (*grey sold line*). The Cuzzi et al. (1993) result (*grey dotted line segments*) is valid for t small compared to the eddy and stopping times, but does not describe diffusion over long times.

To better understand the Cuzzi et al.'s (1993) result for Sc, and why it appears in the geophysical literature as well, we define diffusion coefficients for arbitrary time, $D_{p,g}(t) = \int_0^\tau \langle u_{p,g}(\tau)u_{p,g}(0)\rangle\, d\tau$, which evaluate to (see also Fan and Zhu, 1998):

$$D_p(t) = \frac{\langle u_g^2\rangle t_{eddy}}{t_{stop}^2 - t_{eddy}^2}\Big(t_{stop}^2\big[1-\exp(-t/t_{stop})\big] - t_{eddy}^2\big[1-\exp(-t/t_{eddy})\big]\Big), \tag{16}$$

$$D_g(t) = \langle u_g^2\rangle t_{eddy}\big[1-\exp(-t/t_{eddy})\big]. \tag{17}$$

The short time limit, $t \ll t_{stop}, t_{eddy}$, recovers the Cuzzi et al.'s (1993) result while the long time limit produces the diffusion result, as demonstrated graphically in Fig. 2. The short time limit is of interest in laboratory experiments and in some geophysical contexts for the dynamics internal to the largest eddies. Astrophysicists however are normally interested in the evolution of protoplanetary disks over many eddy times. Furthermore, the early phase of turbulent mixing does not describe diffusion *per se* since separations grow linearly in time, not as $\sqrt{t}$.

Schräpler and Henning (2004) reproduce the Schmidt number result of Cuzzi et al. (1993) by alternate methods, specifically a mean field theory approach, and they also neglect orbital dynamics. The source of the discrepancy with our result is more subtle in this case, but it comes down to their choice of a (second order) closure approximation. A more accurate modeling of the correlation time with their approach should give agreement with our work (Schräpler, personal communication). In any event simple physical arguments should remove any doubt that our result (actually the classic Hinze–Tchen result) gives the correct particle diffusivity for the limiting case of no orbital dynamics.

Another result for Schmidt number, $Sc_{\rm Saf} = (1 + St)^2$ has been attributed to Safronov (1969), originally by Cuzzi et al. (1993). We find no such claim in Safronov (1969). Cuzzi et al.'s (1993) attribution of this result is apparently due to an extension of Safronov's (1969) theory, which itself contains errors. Specifically, Safronov (1969) gives $\delta V_{\rm p} \approx \delta V_{\rm g}/(1 + St)$, which is incorrect. If this is inserted in Eq. (15), it yields the aforementioned expression for $Sc_{\rm Saf}$. The apparent similarity to our result with orbital effects [Eq. (5) with $\tau_{\rm s}$ and St switched] is illusory.

We are thus fully confident that turbulent particle diffusion is independent of St in the absence of orbital effects, and for the simple turbulence models considered. This comparison is intended to give confidence in our methods and clarify a confusing field, not to denigrate these important works.

4.2. Vertical oscillations

We now modify the Langevin equation to include the vertical component of the Keplerian gravitational field:

$$\frac{{\rm d}w_{\rm p}}{{\rm d}t} = -\Omega^2 z_{\rm p} + \frac{w_{\rm g}(t) - w_{\rm p}}{t_{\rm stop}}, \tag{18}$$

where $w_{\rm p} = {\rm d}z_{\rm p}/{\rm d}t$ is the vertical particle velocity and $w_{\rm g}$ the vertical turbulent forcing, which obeys the power spectrum of Eq. (9).[5] Equation (18) describes a damped oscillator that is stochastically forced. The Fourier response of the particle velocity

$$\hat{w}_{\rm p} = \frac{\omega}{\omega + \imath t_{\rm stop}(\Omega^2 - \omega^2)} \hat{w}_{\rm g} \tag{19}$$

gives the squared random velocities as:

$$\begin{aligned}\langle w_{\rm p}^2 \rangle &= \int_{-\infty}^{\infty} {\rm d}\omega\, \hat{E}_{\rm g}(\omega) \frac{|\hat{w}_{\rm p}|^2}{|\hat{w}_{\rm g}|^2} \\ &= \frac{\langle w_{\rm g}^2 \rangle}{1 + \tau_{\rm s}/\tau_{\rm e} + \tau_{\rm s}\tau_{\rm e}} = \frac{\langle w_{\rm g}^2 \rangle}{1 + St(1 + \tau_{\rm e}^2)},\end{aligned} \tag{20}$$

which reduces to the $\Omega = 0$ result of Eq. (13) for eddies much faster than the orbital time. Fig. 3 plots the vertical RMS particle velocities from the square root of Eq. (20). A physical explanation for the large $\tau_{\rm e}$ behavior follows in Section 4.2.2. The limiting forms of Eq. (20) (as well as Eq. (21) below) are presented in Table 1 for each region in Fig. 1.

The particle scale height, $H_{\rm p}$, plotted in Fig. 4, is calculated using $\hat{z}_{\rm p} = \imath \hat{w}_{\rm p}/\omega$ as:

$$H_{\rm p}^2 = \int_{-\infty}^{\infty} {\rm d}\omega\, |\hat{z}_{\rm p}|^2 \frac{\hat{E}_{\rm g}(\omega)}{|\hat{w}_{\rm g}|^2} = \frac{D_{{\rm g},z}}{\Omega\tau_{\rm s}} \frac{1}{\xi(\tau_{\rm s}, \tau_{\rm e})}, \tag{21}$$

$$\xi \equiv 1 + \frac{\tau_{\rm s}\tau_{\rm e}^2}{\tau_{\rm s} + \tau_{\rm e}} = 1 + \frac{St\tau_{\rm e}^2}{1 + St}, \tag{22}$$

using $D_{{\rm g},z} = \langle w_{\rm g}^2 \rangle t_{\rm eddy}$. We compare our result with the standard value derived by Dubrulle et al. (1995) for tightly coupled particles and by Carballido et al. (2006) for loose coupling

$$H_{\rm p}^{\rm (std)} = \sqrt{\frac{D_{{\rm g},z}}{\Omega\tau_{\rm s}}} = \sqrt{\frac{\alpha_z}{\tau_{\rm s}}} H_{\rm g}, \tag{23}$$

where $\alpha_z \equiv D_{{\rm g},z}/(H_{\rm g}^2\Omega)$ is a dimensionless parameter for turbulent diffusion,[6] and $H_{\rm g} = c_{\rm g}/\Omega$ is the gas scale height. Equation (21) reduces to Eq. (23) when $\xi \to 1$, i.e., for $\tau_{\rm e} \ll {\rm Max}(1, 1/\tau_{\rm s})$ as in regions I, II, III and VII of Fig. 1. A phys-

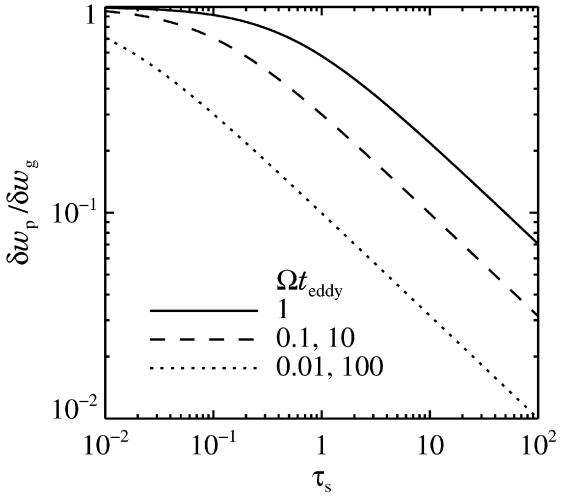

Fig. 3. Vertical RMS speeds of particles, relative to gas turbulence, vs dimensionless particle stopping time for several choices of the eddy turnover time, from Eq. (20). Stirring is most effective for $\tau_{\rm s} \ll 1$ and $\tau_{\rm e} \approx 1$. For large $\tau_{\rm s}$ and/or smaller $\tau_{\rm e}$, particles decouple from eddies. At large $\tau_{\rm e}$ rapid orbital oscillations cancel the kick from eddies, see Section 4.2.2.

Table 1
Summary of results and ordering of timescales by region in Fig. 1

Region	Timescales	$D_{{\rm p},x}/D_{{\rm g},x}$[a]	$H_{\rm p}/H_{\rm g}$[b]	$\delta u_{\rm p}/\delta u_{\rm g}$[c]	$\delta w_{\rm p}/\delta w_{\rm g}$[c]
I	$\tau_{\rm s} < \tau_{\rm e} < 1$	1	$\sqrt{\alpha_z/\tau_{\rm s}}$	1	1
II	$\tau_{\rm e} < \tau_{\rm s} < 1$	1	$\sqrt{\alpha_z/\tau_{\rm s}}$	$\sqrt{\tau_{\rm e}/\tau_{\rm s}}$	$\sqrt{\tau_{\rm e}/\tau_{\rm s}}$
III	$\tau_{\rm e} < 1 < \tau_{\rm s}$	$4/\tau_{\rm s}^2$	$\sqrt{\alpha_z/\tau_{\rm s}}$	$\sqrt{5\tau_{\rm e}/2\tau_{\rm s}}$	$\sqrt{\tau_{\rm e}/\tau_{\rm s}}$
IV	$1 < \tau_{\rm e} < \tau_{\rm s}$	$4/\tau_{\rm s}^2$	$\sqrt{\alpha_z/\tau_{\rm s}\tau_{\rm e}^2}$	$\sqrt{5/2\tau_{\rm s}\tau_{\rm e}}$	$1/\sqrt{\tau_{\rm s}\tau_{\rm e}}$
V	$1 < \tau_{\rm s} < \tau_{\rm e}$	$4/\tau_{\rm s}^2$	$\sqrt{\alpha_z/\tau_{\rm s}^2\tau_{\rm e}}$	$2/\tau_{\rm s}$[d]	$1/\sqrt{\tau_{\rm s}\tau_{\rm e}}$[d]
VI	$\tau_{\rm s} < 1 < \tau_{\rm s}^{-1} < \tau_{\rm e}$	1	$\sqrt{\alpha_z/\tau_{\rm s}^2\tau_{\rm e}}$	1[d]	$1/\sqrt{\tau_{\rm s}\tau_{\rm e}}$[d]
VII	$\tau_{\rm s} < 1 < \tau_{\rm e} < \tau_{\rm s}^{-1}$	1	$\sqrt{\alpha_z/\tau_{\rm s}}$	1	1

Note. Results for particle radial diffusion ($D_{{\rm p},x}$), scale height ($H_{\rm p}$), and radial ($\delta u_{\rm p}$) and azimuthal ($\delta w_{\rm p}$) RMS velocities from Eqs. (36), (21), (33a), and (20) in the appropriate limiting cases. The in-plane results (diffusion and radial velocity) assume isotropic radial and azimuthal speeds.

[a] Regions II, III, IV, and V, differ from the previous result for $D_{\rm p}$ in Eq. (15) which gave $1/St$ for II, III, and IV, and 1 for region V.

[b] Regions IV, V, and VI all give a thinner particle scale height than the standard result $\sqrt{\alpha_z/\tau_{\rm s}}$ in Eq. (23).

[c] Regions IV and V for radial speeds and Regions IV, V and VI for vertical speeds (all of which have long eddy times) differ from the standard result $1/\sqrt{1 + St}$ from Eq. (13).

[d] The radial and azimuthal speeds have a different scaling in regions V and VI because the eddy time is longer than the vertical settling time.

[5] With $\langle w_{\rm g}^2 \rangle$ instead of $\langle u_{\rm g}^2 \rangle$.

[6] Note that this is not the same α-parameter used for diffusion of angular momentum, and that turbulence is subsonic for $\alpha_z/\tau_{\rm e} = \langle w_{\rm g}^2 \rangle / c_{\rm g}^2 < 1$.

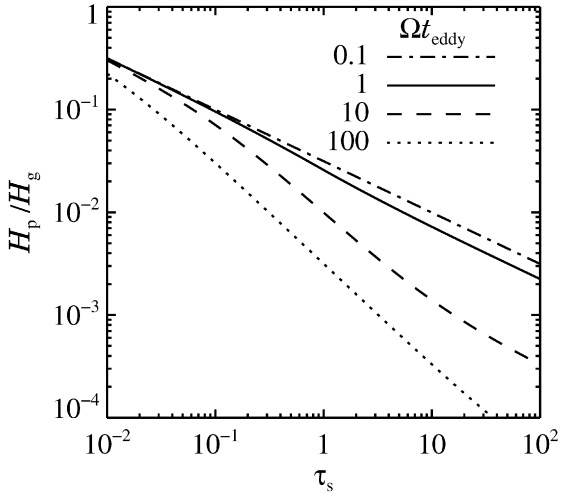

Fig. 4. Particle scale height relative to gas vs stopping time for several values of the eddy time with turbulent diffusion at a level of $\alpha_z \equiv D_{{\rm g},z}/(H_{\rm g}^2\Omega) = 10^{-3}$. The particle layer becomes thinner for increasing particle stopping time. The layer also becomes thinner for eddy times longer than the orbital time and the settling time, $1/(\Omega\tau_{\rm s})$, due to the cancellation of kicks as in Fig. 3.

ical description of the large eddy time behavior follows. For $\tau_{\rm e} = 1$ our result becomes:

$$H_{\rm p}^{\tau_{\rm e}=1} = \sqrt{\frac{D_{{\rm g},z}}{\Omega\tau_{\rm s}}}\sqrt{\frac{1+\tau_{\rm s}}{1+2\tau_{\rm s}}}. \tag{24}$$

The maximum discrepancy of $\sqrt{2}$ for $\tau_{\rm s} \gg 1$ is not very significant.

Since particles are confined to a vertical potential well, we cannot measure long term spatial diffusion as in Eqs. (11a)–(11c). We show in Section 3.3 that the particle diffusivity required to maintain $H_{\rm p}$ agrees with the physical estimate of Sc in Eq. (5).

4.2.1. Applications and extensions

The ratio between velocity dispersion and scale height,

$$\frac{\langle w_{\rm p}^2\rangle^{1/2}}{H_{\rm p}} = \Omega\sqrt{\frac{St}{1+St}}, \tag{25}$$

reduces to the Keplerian oscillation frequency for loose coupling to eddies, $St \gg 1$. One might have naively guessed that the criterion would be $\tau_{\rm s} \gg 1$, but see Section 3 and Section 4.2.2 for explanations of the surprising behavior in regions II and V, respectively. For $St \ll 1$, collision rates will fall below the usual disk estimate of Ω times the vertical optical depth, $\tau_{\rm p}$ by $\sqrt{St}$, since the decrease in density (with larger $H_{\rm p}$) is not matched by the increase in RMS speeds. Since particle relative speeds are reduced below RMS speeds by a factor $\sqrt{St}$ for $St \ll 1$ (Völk et al., 1980) the collision rate is

$$t_{\rm coll}^{-1} \sim \Omega\tau_{\rm p}\frac{St}{1+St} \tag{26}$$

for equal size particles, assuming that vertical speeds are at least comparable to in-plane motions. Note that this result is independent of the strength of turbulence (though for different particle sizes turbulence must compete with differential aerodynamic drift).

We also compare the vertical settling speed for $\tau_{\rm s} \ll 1$: $w_{\rm sett} = |g_z|t_{\rm stop} \approx \Omega\tau_{\rm s}H_{\rm p}$ to RMS particle speeds:

$$\frac{w_{\rm sett}}{\langle w_{\rm p}^2\rangle^{1/2}} \approx \sqrt{(\tau_{\rm e}+\tau_{\rm s})\tau_{\rm s}}. \tag{27}$$

For $\tau_{\rm s} \ll 1$, the above is a small quantity (except for the extreme case of region VI, where $t_{\rm eddy} > t_{\rm sett}$, see Section 4.2.2), so that random motions exceed the ordered settling that would occur without turbulence.

We have assumed that both the particle stopping time, and the turbulent spectrum are independent of height above the midplane. This restricts the range of validity of our results to $H_{\rm p} < H_{\rm g}$ so that gas density, $\rho_{\rm g}$, is roughly constant. In stratified models, $H_{\rm p} \leqslant H_{\rm g}$ is imposed by the hypothesis that the quantity diffused by turbulence is not the absolute particle density, but the particle concentration relative to gas[7] (Dubrulle et al., 1995, their Eq. (28)). We suggest

$$\frac{H_{\rm p}}{H_{\rm g}} \approx \sqrt{\frac{\alpha_z}{\alpha_z+\tau_{\rm s}}}\xi^{-1/2} < 1 \tag{28}$$

as a simple way to enforce the restriction $H_{\rm p} < H_{\rm g}$.

The approximation (that turbulence acts to smooth concentration gradients) does not hold for larger particles, which move through the gas. In practice this distinction is not important since $H_{\rm p}/H_{\rm g} \approx \sqrt{\alpha/\tau_{\rm s}} \ll 1$ for $\tau_{\rm s} \gg 1$ and $\alpha \lesssim 1$. Thus heavy particles always settle within $H_{\rm g}$ in any event. See Section 5 for more on the diffusion of heavy particles.

4.2.2. Physical understanding of vertical forcing for large $\tau_{\rm e}$

In Section 3 we provide physical explanations for the velocity dispersion, diffusion, and scale height of particles in the $\tau_{\rm e} \ll 1$ limit, i.e., the lower half of Fig. 1. We now consider $\tau_{\rm e} \gg 1$, which is considerably more complex, particularly in regions V and VI where $t_{\rm eddy} > t_{\rm sett}$. We denote the particle and gas RMS speeds as $\delta w_{\rm p}$ and $\delta w_{\rm g}$, respectively.

We first note that region VII behaves just as region I since particles are tightly coupled to both orbits and eddies, and the eddy time is shorter than the particle settling time. Thus $\delta w_{\rm p} \sim \delta w_{\rm g}$ and $H_{\rm p} \sim \sqrt{D_{\rm g}/(\Omega\tau_{\rm s})}$ in agreement with Eqs. (20) and (21), in the limits $St \ll 1$ and $St\tau_{\rm e}^2 = t_{\rm eddy}/t_{\rm sett} \ll 1$.

Region IV has loose particle coupling to eddies and gas orbits, and long eddy times. As in regions II and III, the velocity grows by a random walk. However since $t_{\rm eddy} \gg \Omega^{-1}$, the kick from an eddy is largely canceled by the many vertical oscillations in an eddy time. Thus the kick is only received over the last orbital cycle, $V_{\rm kick} \sim \delta w_{\rm g}/\tau_{\rm s}$. After $N = t_{\rm stop}/t_{\rm eddy}$ kicks the velocity saturates with $\delta w_{\rm p} \sim V_{\rm kick}\sqrt{N} = \delta w_{\rm g}/\sqrt{\tau_{\rm s}\tau_{\rm e}}$. Vertical oscillations with loose orbital coupling then gives $H_{\rm p} = \delta w_{\rm p}/\Omega$. Equations (20) and (21) agree with these estimates in the relevant $St \gg 1$, $St\tau_{\rm e}^2 = St\tau_{\rm s} \gg 1$ limit. As a consistency

[7] See also Chamberlain and Hunten (1987, p. 90) for the same approximation in planetary atmospheres. The assumption is that turbulent diffusion mimics molecular diffusion, which is driven by concentration gradients [and also thermal gradients, see Landau and Lifshitz (1959, Eq. (58.14))].

check, note that $H_p/\ell_{eddy} \sim 1/\sqrt{\tau_s\tau_e^3} \ll 1$ so particle oscillations easily fit within a single large eddy.

Since eddy times exceed settling times in regions V and VI, H_p is not determined by the usual diffusion arguments. Instead long-lived eddies suspend particles at $H_p \sim \delta w_g/(\Omega\tau_s)$, by force balance between gravity, $\Omega^2 H_p$, and drag, $\delta w_g/t_{stop}$, in agreement with Eq. (21) for $St \ll 1$ and $\tau_s^2/St = \tau_s\tau_e \gg 1$ (regions V and VI). Hubbard and Blackman (2006) give similar arguments, but without the caveats on the ordering of timescales. Though "pinned" by slow eddies, particles will be stirred by faster eddies with $t'_{eddy} \sim t_{sett} \ll t_{eddy}$, and a speed $\delta w'_g \sim \delta w_g\sqrt{t'_{eddy}/t_{eddy}}$ (the transformation of the Kolmogorov relation $v_\ell \propto \ell^{1/3}$ to the time domain). For $\tau_s \ll 1$ (region VI), $t'_{eddy} \sim t_{sett} = (\Omega\tau_s)^{-1}$, and tight coupling to these slower eddies gives $\delta w_p \sim \delta w'_g \sim \delta w_g/\sqrt{\tau_s\tau_e}$. For $\tau_s \gg 1$ (region V), $t'_{eddy} \sim t_{sett} = t_{stop}$, and the relevant eddy speed is $\delta w'_g \sim \delta w_g\sqrt{St}$. However the fast oscillations give an effective kick duration of Ω^{-1} as in region IV, and $\delta w_p \sim \delta w'_g/\tau_s \sim \delta w_g/\sqrt{\tau_s\tau_e}$. There is no accumulation of kicks since each eddy lasts a stopping time, $t'_{eddy} \sim t_{stop}$. Equation (20) confirms, in the $St = \tau_s/\tau_e \ll 1$ and $\tau_s\tau_e \gg 1$ limits, that $\delta w_p \sim \delta w_g/\sqrt{\tau_s\tau_e}$ in regions V and VI as shown in Table 1.

These physical arguments justify our new results for the scaling of particle scale height and vertical RMS speeds in the large τ_e regime.

4.3. Epicyclic oscillations

We now treat the turbulent forcing of epicyclic oscillations. For small eccentricities, we consider the locally Cartesian radial, x_p, and azimuthal, y_p, positions relative to a guiding center with Keplerian orbital frequency, Ω. Hill's linearized equations of motion with gas drag read:

$$\dot{x}_p = u_p, \tag{29a}$$

$$\dot{y}_p = v_p - (3/2)\Omega x_p, \tag{29b}$$

$$\dot{u}_p = 2\Omega v_p + \frac{u_g(t) - u_p}{t_{stop}}, \tag{29c}$$

$$\dot{v}_p = -\frac{\Omega u_p}{2} + \frac{v_g(t) - v_p}{t_{stop}}, \tag{29d}$$

where we measure azimuthal velocities, v_p, relative to local Keplerian shear. We ignore any time-steady gas velocities, such as pressure-supported sub-Keplerian rotation of the gas would provide.[8]

We assign the same temporal turbulent spectrum, $\hat{P}(\omega)$ as Eq. (9). For generality we will keep the amplitudes of the radial, azimuthal, and correlated gas forcing; $\langle u_g^2\rangle$, $\langle v_g^2\rangle$, and $\langle u_g v_g\rangle$; independent in many expressions to allow comparison with numerical simulations. Equation (B.1) gives a model to relate these quantities.

[8] The resulting (locally constant) drift of particles relative to gas can still be included with a correction to the eddy time from Eq. (60).

4.3.1. Velocity response

The Fourier responses of particle velocities to turbulent forcing are:

$$\hat{u}_p = \frac{(1 - \imath\nu_s)\hat{u}_g + 2\tau_s\hat{v}_g}{(1 - \imath\nu_s)^2 + \tau_s^2}, \tag{30a}$$

$$\hat{v}_p = \frac{-(\tau_s/2)\hat{u}_g + (1 - \imath\nu_s)\hat{v}_g}{(1 - \imath\nu_s)^2 + \tau_s^2}, \tag{30b}$$

where $\nu_s \equiv \omega t_{stop}$. The squared Fourier amplitudes and correlations read:

$$|\hat{u}_p|^2 = \frac{1}{d(\omega)}\Bigg[\big(1+\nu_s^2\big)|\hat{u}_g|^2 + 4\tau_s^2|\hat{v}_g|^2 + 4\tau_s\frac{\hat{u}_g\hat{v}_g^* + \hat{u}_g^*\hat{v}_g}{2}\Bigg], \tag{31a}$$

$$|\hat{v}_p|^2 = \frac{1}{d(\omega)}\Bigg[\frac{\tau_s^2}{4}|\hat{u}_g|^2 + \big(1+\nu_s^2\big)|\hat{v}_g|^2 - \tau_s\frac{\hat{u}_g\hat{v}_g^* + \hat{u}_g^*\hat{v}_g}{2}\Bigg], \tag{31b}$$

$$\frac{\hat{u}_p\hat{v}_p^* + \hat{u}_p^*\hat{v}_p}{2} = \frac{1}{d(\omega)}\Bigg[-\frac{\tau_s}{2}|\hat{u}_g|^2 + 2\tau_s|\hat{v}_g|^2 + \big(1+\nu_s^2-\tau_s^2\big)\frac{\hat{u}_g\hat{v}_g^* + \hat{u}_g^*\hat{v}_g}{2}\Bigg], \tag{31c}$$

where $d(\omega) = [1 + \nu_s^2 + \tau_s^2]^2 - 4(\nu_s\tau_s)^2$. In Eqs. (31a)–(31b), terms in the numerator $\propto\imath\nu_s(\hat{u}_g\hat{v}_g^* - \hat{u}_g^*\hat{v}_g)$ are dropped since they are odd in ν_s and will vanish on integration over frequency.

Since the amplitudes have the form, e.g., $|\hat{u}_p|^2 = a|\hat{u}_g|^2 + b|\hat{v}_g|^2 + c(\hat{u}_g\hat{v}_g^* + \hat{u}_g^*\hat{v}_g)/2$, we generalize the particle power spectrum from Eq. (12) to:

$$\hat{E}_{p,x}(\omega) = \big[a\langle u_g^2\rangle + b\langle v_g^2\rangle + c\langle u_g v_g\rangle\big]\hat{P}(\omega) \tag{32}$$

and similarly for the y power and x–y correlations. The particle energies are derived as before, e.g., $\langle u_p^2\rangle = \int_{-\infty}^{\infty}\hat{E}_{p,x}\,d\omega$, to give:

$$\langle u_p^2\rangle = \frac{1}{d_2}\Big\{\big[1 + St\big(1+\tau_s^2/2\big)\big]\langle u_g^2\rangle + 2\tau_s^2(2+St)\langle v_g^2\rangle + 2\tau_s(2+St)\langle u_g v_g\rangle\Big\}, \tag{33a}$$

$$\langle v_p^2\rangle = \frac{1}{d_2}\Bigg\{\frac{\tau_s^2(2+St)}{8}\langle u_g^2\rangle + \big[1 + St\big(1+\tau_s^2/2\big)\big]\langle v_g^2\rangle - \tau_s(2+St)\langle u_g v_g\rangle/2\Bigg\}, \tag{33b}$$

$$\langle u_p v_p\rangle = \frac{1}{d_2}\Bigg\{-\frac{\tau_s(2+St)}{4}\langle u_g^2\rangle + \tau_s(2+St)\langle v_g^2\rangle + \big(1 + St - \tau_s^2\big)\langle u_g v_g\rangle\Bigg\}, \tag{33c}$$

where $d_2 \equiv (1+\tau_s^2)[(1+St)^2 + \tau_s^2]$.

Since the expressions are fairly cumbersome it is fruitful to investigate limiting cases. Table 1 lists the limiting forms of $\delta u_p/\delta u_g \equiv (\langle u_p^2\rangle/\langle u_g^2\rangle)^{1/2}$, using the turbulence model in Eq. (B.1) for the other components of gas forcing. For more general analysis, we first consider $\tau_s \ll 1$, i.e., the left half of

Fig. 1. The equations simplify considerably to:

$$\frac{\langle u_p^2\rangle}{\langle u_g^2\rangle} = \frac{\langle v_p^2\rangle}{\langle v_g^2\rangle} = \frac{\langle u_p v_p\rangle}{\langle u_g v_g\rangle} = \frac{1}{1+St}. \tag{34}$$

There is no epicyclic motion since particles are tightly coupled to gas orbits, and the response scales directly with the forcing.[9] The scaling with St agrees with Eq. (13) in the absence of orbital dynamics.

Next consider the limit of short eddy times, $\tau_e \ll 1$ and $St \gg 1$ in regions II and III, which we will compare to our Fokker–Planck results in Section 5. Here the particle response is

$$\langle u_p^2\rangle = \frac{(1+\frac{\tau_s^2}{2})\langle u_g^2\rangle + 2\tau_s^2\langle v_g^2\rangle + 2\tau_s\langle u_g v_g\rangle}{St(1+\tau_s^2)} = \frac{\langle u_g^2\rangle}{St}\frac{1+5\tau_s^2/2}{1+\tau_s^2}, \tag{35a}$$

$$\langle v_p^2\rangle = \frac{\frac{\tau_s^2}{8}\langle u_g^2\rangle + (1+\frac{\tau_s^2}{2})\langle v_g^2\rangle - \tau_s\langle u_g v_g\rangle/2}{St(1+\tau_s^2)} = \frac{\langle u_g^2\rangle}{St}\frac{1+5\tau_s^2/8}{1+\tau_s^2}, \tag{35b}$$

$$\langle u_p v_p\rangle = \frac{-\frac{\tau_s}{4}\langle u_g^2\rangle + \tau_s\langle v_g^2\rangle + \langle u_g v_g\rangle}{St(1+\tau_s^2)} = \frac{\langle u_g^2\rangle}{St}\frac{3\tau_s/4}{1+\tau_s^2}, \tag{35c}$$

where the final equalities assume isotropic turbulence with $\langle u_g^2\rangle = \langle v_g^2\rangle$ and ignore $\langle u_g v_g\rangle$, consistent with Eq. (B.1).[10] For small τ_s Eqs. (35a)–(35c) recover the $St \gg 1$ limit of Eq. (34). For $\tau_s \gg 1$ we recover epicyclic motion. The radial RMS speeds are twice the azimuthal RMS speeds, whether the forcing is radial, azimuthal or combined.[11] Equation (35c) shows that radial turbulent forcing produces a negative $\langle u_p v_p\rangle$, i.e., inward transport of particle angular momentum. Azimuthal forcing has the opposite sign, and dominates for our assumption of isotropy.

Region IV exhibits epicyclic oscillations since Ω^{-1} is the most rapid timescale. The ratio of RMS particle to turbulent speeds scale at $\sqrt{St}/\tau_s = 1/\sqrt{\tau_s\tau_e}$ in agreement with the physical arguments in Section 4.2.2. Region V is rather complicated since even though $\tau_s > 1$ particles do not complete epicycles as they are tightly coupled to eddies, $St < 1$.

4.3.2. *Numerical evaluation and visual interpretation of velocities*

Fig. 5 plots RMS velocities and velocity correlations from the (square root of) Eqs. (33a)–(33c) for the turbulence model of Eq. (B.1). This model assumes that velocities are isotropic,

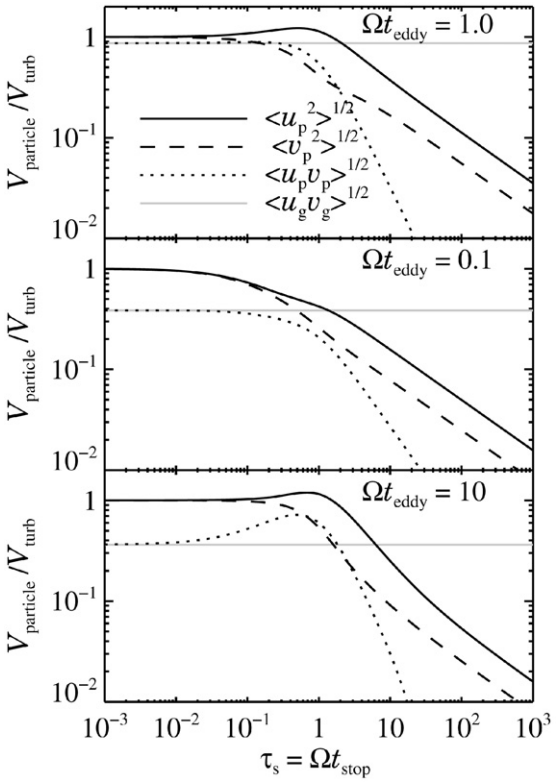

Fig. 5. Particle RMS speeds (radial, *solid curves*; azimuthal, *dashed curves*), relative to the turbulent RMS speed, $V_{turb} = \sqrt{\langle u_g^2 + v_g^2\rangle/2}$, versus stopping time for three different values of the eddy time ($t_{eddy} = 1.0/\Omega$, $0.1/\Omega$, and $10.0/\Omega$ in the *top, middle*, and *bottom* panels). The (square root of) the particle velocity correlations is plotted (*dotted curves*). The turbulent gas correlations (*grey lines*) transport angular momentum, but have a small effect on the particle velocities (and only near $\tau_s = 1$). See Section 4.3.2 for discussion.

$\langle u_g^2\rangle = \langle v_g^2\rangle$, and estimates a maximum correlation, $\langle u_g v_g\rangle$ (grey curves). Speeds are normalized to the characteristic turbulent speed, $V_{turb} \equiv (\langle u_g^2 + v_g^2\rangle/2)^{1/2}$, and results are shown for $\tau_e = 0.1$, 1.0, and 10.0 (middle, top, and bottom panels respectively).

For $\tau_s \ll 1$, particle RMS speeds simply follow the gas forcing, here the isotropic value V_{turb}. For $\tau_s \gg 1$, the RMS speeds fall as $\tau_s^{-1/2}$, and the ratio of radial (solid curves) to azimuthal (dashed curves) speeds approaches the epicyclic value of two. As τ_e deviates from unity (becoming either larger or smaller) the RMS speeds at large τ_s drop roughly as $\sqrt{\tau_e/(1+\tau_e^2)}$. Similar behavior was seen for vertical speeds in Fig. 3. Thus the RMS velocities of large particle are a good indicator of whether the eddy time differs from unity.

The speeds near $\tau_s \approx 1$ are sensitive to the eddy time and the $\langle u_g v_g\rangle$ correlations. For $\tau_e = 1.0$, the "bump" in radial speed near $\tau_s = 1$ is due to the high value of $\langle u_g v_g\rangle$ (otherwise the radial velocities would be flat up to $\tau_s = 1$). For $\tau_e = 0.1$ there is a noticeable drop in speeds by $\tau_s = 1$, because with $St = \tau_s/\tau_e = 10$ particles have begun to decouple from eddies. For $\tau_e = 10$ the radial velocity bump exists even without gas correlations, which are weak here. The difference in speeds near $\tau_s \approx 1$ discriminates between large and small eddy times. We emphasize that the turbulent transport of angular momentum by Reynolds stresses $\langle u_g v_g\rangle$ has only a small effect on particle speeds, and then only near $\tau_s \approx 1$.

[9] A possible exception occurs if, e.g., the azimuthal turbulent forcing is much stronger than the radial.

[10] We have dropped a term $-\tau_s\tau_e\langle u_g v_g\rangle$ from the numerator of the middle expression in Eq. (35c) because it is always smaller than the other terms in the numerator for $\tau_e \ll 1$.

[11] Random velocities are measured relative to the local circular speed. Relative to a fixed guiding center the elongation of epicycles is opposite; azimuthal speeds are twice radial (Binney and Tremaine, 1987).

4.3.3. Radial particle diffusion

Radial diffusion[12] of particles can be calculated as in Eq. (14) to give

$$D_{\mathrm{p},x} = \int_0^\infty \mathrm{d}\tau \int_{-\infty}^{\infty} \mathrm{d}\omega\, \hat{E}_{\mathrm{p},x} e^{-\imath\omega t} = \pi \hat{E}_{\mathrm{p}}(0)$$
$$= t_{\mathrm{eddy}} \frac{\langle u_{\mathrm{g}}^2\rangle + 4\tau_{\mathrm{s}}^2\langle v_{\mathrm{g}}^2\rangle + 4\tau_{\mathrm{s}}\langle u_{\mathrm{g}} v_{\mathrm{g}}\rangle}{(1+\tau_{\mathrm{s}}^2)^2}. \quad (36)$$

The $\tau_{\mathrm{s}} \ll 1$ limit recovers the result of Eq. (14) that particles of any size diffuse as a gas tracer *when orbital motions are neglected*. Azimuthal forcing has a negligible effect since tightly coupled particles quickly adjust to the local orbital speed. For $\tau_{\mathrm{s}} \gg 1$, radial diffusion is dominated by the azimuthal forcing, $D_{\mathrm{p},x} = 4\langle v_{\mathrm{g}}^2\rangle t_{\mathrm{eddy}}/\tau_{\mathrm{s}}^2$, since angular momentum perturbations are needed to change semimajor axes. The scaling for loose coupling agrees with the estimate of Eq. (4). Correlated gas fluctuations, $\langle u_{\mathrm{g}} v_{\mathrm{g}}\rangle$, are a minor correction to radial particle diffusion, and only near $\tau_{\mathrm{s}} \sim 1$ (as with the velocities). The limiting forms of Eq. (36) are listed in Table 1 for the turbulence model in Eq. (B.1).

The radial Schmidt number can be expressed for homogeneous isotropic turbulence $\langle u_{\mathrm{g}}^2\rangle = \langle v_{\mathrm{g}}^2\rangle$, $\langle u_{\mathrm{g}} v_{\mathrm{g}}\rangle = 0$ as:

$$Sc_x \equiv \frac{D_{\mathrm{g},x}}{D_{\mathrm{p},x}} = \frac{(1+\tau_{\mathrm{s}}^2)^2}{1+4\tau_{\mathrm{s}}^2}, \quad (37)$$

where $D_{\mathrm{g},x} = \langle u_{\mathrm{g}}^2\rangle t_{\mathrm{eddy}}$. This is consistent with, but provides order unity corrections to the rough estimate in Eq. (5). It is interesting that this result is completely independent of the eddy time.

Fig. 6 plots the radial particle diffusion, $D_{\mathrm{p},x}$, relative to the diffusion of gas, $D_{\mathrm{g},x}$. The black curves use Eq. (36) and the turbulence model in Eq. (B.1). Since the correlations $\langle u_{\mathrm{g}} v_{\mathrm{g}}\rangle$ are a minor contribution, the black curves overlap with each other and with Eq. (37) (or rather its inverse, not plotted). The overlap only occurs because $\langle u_{\mathrm{g}}^2\rangle = \langle v_{\mathrm{g}}^2\rangle$ in all cases. If the velocities were anisotropic then the diffusion for $\tau_{\mathrm{s}} \gg 1$ would vary as $\langle v_{\mathrm{g}}^2\rangle/\langle u_{\mathrm{g}}^2\rangle$, i.e. $D_{\mathrm{p},x}$ would be larger (smaller) if azimuthal kinetic energy exceeds (falls below) the radial contribution.

The Cuzzi et al.'s (1993) value for Sc, Eq. (15), is plotted for reference (dotted grey curve). The physical shortcomings of this result (neglect of epicyclic oscillations and particle mean free path) are discussed in Section 4.1.1. While the Cuzzi et al.'s (1993) value overpredicts diffusion for very large particles $\tau_{\mathrm{s}} \gg 1$, it tends to underpredict diffusion for marginal coupling, $\tau_{\mathrm{s}} \sim 1$.

4.3.4. Monte Carlo diffusion simulation

Testing our results with detailed turbulence simulations (or experiments) is beyond the scope of this paper. Instead we visualize the combination of diffusion and epicyclic motion with the Monte Carlo simulation shown in Fig. 7. We integrated Eqs. (29a)–(29d) numerically, with $\tau_{\mathrm{s}} = 10^2$ and $\tau_{\mathrm{e}} = 10^{-2}$ (region III of Fig. 1). As a crude model for the forcing by the gas, we set $u_{\mathrm{g}}(t) = \pm 1$ and $v_{\mathrm{g}}(t) = \pm 1$ for a time approximately t_{eddy}. More precisely, we updated u_{g} and v_{g} at every time step with probability $\mathrm{d}t/t_{\mathrm{eddy}}$, where $\mathrm{d}t$ is the time step, and the decision to update was implemented with a random number generator. If an update was warranted, the sign of u_{g} and of v_{g} was each randomly selected. The three curves in the figure show three realizations of the random number generator. For the oscillation amplitudes, Eq. (35a) predicts that $\langle u_{\mathrm{p}}^2\rangle = (5/2)\langle u_{\mathrm{g}}^2\rangle\tau_{\mathrm{e}}/\tau_{\mathrm{s}} = (0.016)^2$, implying that the peak-to-peak amplitude of x should be $0.016\sqrt{8}\Omega^{-1} =$

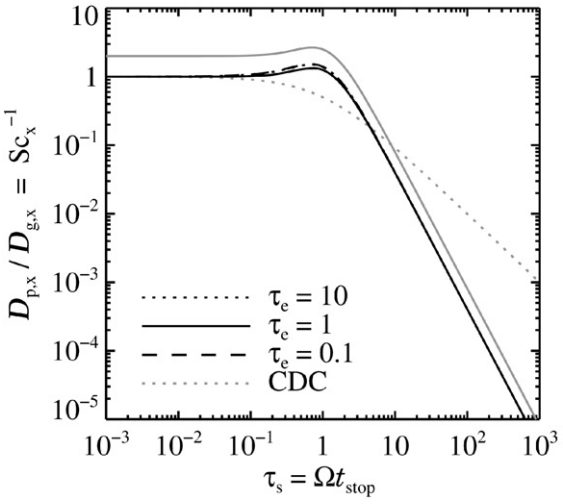

Fig. 6. Radial particle diffusion, relative to gas diffusion, versus stopping time. The black curves [from Eqs. (36) and (B.1)] overlap despite different choices of eddy time. For tight coupling ($\tau_{\mathrm{s}} \ll 1$) particles diffuse as effectively as gas. For loose coupling ($\tau_{\mathrm{s}} \gg 1$) particle diffusion falls as τ_{s}^{-2}. The Cuzzi et al.'s (1993) result, $Sc = 1 + St$ with $\tau_{\mathrm{e}} = 1$ (*grey dotted curve*) overestimates the diffusion of large ($\tau_{\mathrm{s}} \gg 1$) particles and slightly underestimates diffusion of marginally coupled solids.

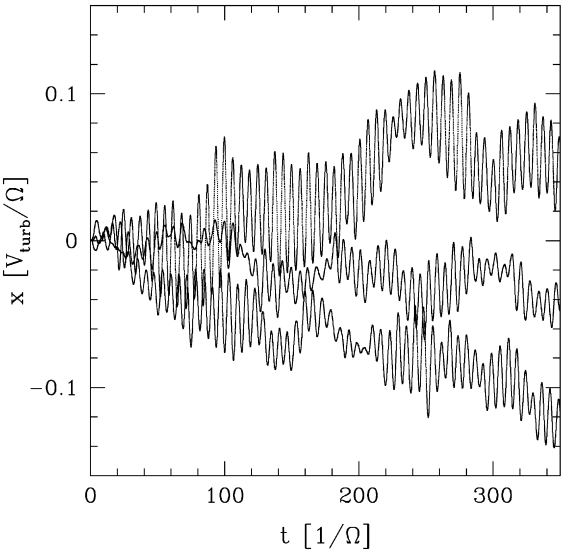

Fig. 7. A Monte Carlo simulation of the radial diffusion of three particles undergoing epicyclic motion with $\tau_{\mathrm{s}} = 10^2$ and $\tau_{\mathrm{e}} = 10^{-2}$. The radial coordinate x is normalized to the RMS turbulent gas speed divided by the Kepler frequency. See Section 4.3.4 for details.

[12] We do not here consider azimuthal diffusion. It is less interesting since orbital shear is much more effective at spreading non-axisymmetric structure.

$0.04\Omega^{-1}$, in agreement with the oscillations seen in the figure. For the diffusion, Eq. (36) predicts the diffusion constant $D_{\mathrm{p},x} = t_{\mathrm{eddy}}(4/\tau_{\mathrm{s}}^2)\langle v_{\mathrm{g}}^2\rangle = \Omega^{-1}(0.002)^2$, implying that $x \simeq (2D_{\mathrm{p},x}t)^{1/2} = \Omega^{-1}0.05$ at $t = 300\Omega^{-1}$, in agreement with the diffusion seen in the figure.

5. Fokker–Planck equation

When the eddy correlation time t_{eddy} is the smallest timescale, the random gas motions give short uncorrelated kicks to the particles which can be described by a Fokker–Planck equation. The Fokker–Planck equation has been used extensively to study Brownian motion (Chandrasekhar, 1943). While the uncorrelated collisions in Brownian motion lead to thermal equipartition, the correlated motion of turbulent eddies excite particles to much higher speeds. Carballido et al. (2006) use the Fokker–Planck technique to study vertical settling. By solving the in-plane Fokker–Planck equation we reproduce the results of Section 4.3 in the small t_{eddy} limit, adding confidence in our results.

It greatly simplifies the analysis to switch to indicial notation, re-writing the equations of motion for a particle given in Eqs. (29a)–(29d) as

$$\frac{\mathrm{d}x_i}{\mathrm{d}t} = u_i - \frac{3}{2}\Omega x_1 \delta_{iy}, \tag{38a}$$

$$\frac{\mathrm{d}u_i}{\mathrm{d}t} = A_{ij}u_j + \frac{u_{\mathrm{g},i}}{t_{\mathrm{stop}}}, \tag{38b}$$

where $i, j \in \{x, y\}$, summation over repeated indices is implied, and

$$A_{ij} \equiv \begin{pmatrix} -t_{\mathrm{stop}}^{-1} & 2\Omega \\ -\Omega/2 & -t_{\mathrm{stop}}^{-1} \end{pmatrix}. \tag{39}$$

We suppress the subscript p from x_i, u_i.

The Fokker–Planck equation for the particle distribution function $f(x_i, u_i, t)$ reads

$$\partial_t f = -\partial_i\left(\frac{\langle\Delta x_i\rangle}{\Delta t} f\right) - \partial_{u_i}\left(\frac{\langle\Delta u_i\rangle}{\Delta t} f\right) + \frac{1}{2}\partial^2_{u_i u_j}\left(\frac{\langle\Delta u_i \Delta u_j\rangle}{\Delta t} f\right) \tag{40}$$

(e.g., Eqs. (8)–(53) in Binney and Tremaine, 1987). The angled brackets denote an ensemble average over the stochastic variable $u_{\mathrm{g},i}$, and $\Delta x_i, \Delta u_i$ denote the change in x_i, u_i over the time interval Δt, in the limit that $\Delta t \to 0$. (To be more precise, Δt must be larger than t_{eddy}, but much smaller than all other timescales.) We have dropped the term containing $\langle\Delta x_i \Delta x_j\rangle/\Delta t$ because, from Eq. (38a), it is proportional to Δt, and hence vanishes for $\Delta t \to 0$. To calculate $\langle\Delta u_i \Delta u_j\rangle/\Delta t$, we may drop the $A_{ij}u_j$ on the right-hand side of Eq. (38b) because it only contributes a term of order Δt to $\langle\Delta u_i \Delta u_j\rangle/\Delta t$; we are left with

$$\Delta u_i = \frac{1}{t_{\mathrm{stop}}}\int_t^{t+\Delta t} u_{\mathrm{g},i}(t')\,\mathrm{d}t', \tag{41}$$

implying

$$\frac{\langle\Delta u_i \Delta u_j\rangle}{\Delta t} = \frac{1}{\Delta t}\frac{2}{t_{\mathrm{stop}}^2}\int_t^{t+\Delta t}\int_t^{t'}\left\langle u_{\mathrm{g},i}(t')u_{\mathrm{g},j}(t'')\right\rangle \mathrm{d}t''\,\mathrm{d}t' = \frac{2t_{\mathrm{eddy}}}{t_{\mathrm{stop}}^2}\langle u_{\mathrm{g},i}u_{\mathrm{g},j}\rangle, \tag{42}$$

in agreement with Eq. (9) of Carballido et al. (2006). The remaining averages are given by Eqs. (38a)–(38b) as

$$\frac{\langle\Delta x_i\rangle}{\Delta t} = \langle u_i\rangle - \frac{3}{2}\Omega\langle x_1\rangle\delta_{iy}, \tag{43a}$$

$$\frac{\langle\Delta u_i\rangle}{\Delta t} = A_{ij}\langle u_j\rangle. \tag{43b}$$

The Fokker–Planck equation then becomes

$$\tilde{\partial}_t f + u_i\partial_i f = -\partial_{u_i}(A_{ij}u_j f) + D_{u_i u_j}\partial^2_{u_i u_j} f, \tag{44}$$

suppressing angled brackets and defining

$$D_{u_i u_j} \equiv \frac{t_{\mathrm{eddy}}}{t_{\mathrm{stop}}^2}\langle u_{\mathrm{g},i}u_{\mathrm{g},j}\rangle \tag{45}$$

as the velocity diffusion, and $\tilde{\partial}_t \equiv \partial_t - (3/2)\Omega x\partial_y$ which reduces to a simple time derivative for an axisymmetric ($\partial_y f = 0$) distribution function.

We solve the Fokker–Planck equation (44) by taking velocity moments, defining the mass per unit area, mean velocity, and peculiar velocity tensors:

$$\Sigma \equiv \int f\,\mathrm{d}u_x\,\mathrm{d}u_y, \tag{46a}$$

$$U_i \equiv \Sigma^{-1}\int u_i f\,\mathrm{d}u_x\,\mathrm{d}u_y, \tag{46b}$$

$$\Pi_{ij} \equiv \Sigma^{-1}\int (u_i - U_i)(u_j - U_j) f\,\mathrm{d}u_x\,\mathrm{d}u_y, \tag{46c}$$

$$\Xi_{ijk} \equiv \Sigma^{-1}\int (u_i - U_i)(u_j - U_j)(u_k - U_k) f\,\mathrm{d}u_x\,\mathrm{d}u_y. \tag{46d}$$

Multiplying Eq. (44) by $\{1, u_i, u_i u_j\}$, and then integrating out u_x, u_y, and y yields

$$\tilde{\partial}_t\Sigma + \partial_i\Sigma U_i = 0, \tag{47a}$$

$$\tilde{\partial}_t U_i + U_j\partial_j U_i = -\Sigma^{-1}\partial_j(\Sigma\Pi_{ij}) + A_{ij}U_j, \tag{47b}$$

$$\tilde{\partial}_t\Pi_{ij} + U_k\partial_k\Pi_{ij} + \Pi_{ik}\partial_k U_j + \Pi_{jk}\partial_k U_i + \Sigma^{-1}\partial_k(\Sigma\Xi_{kij}) = A_{ik}\Pi_{kj} + A_{jk}\Pi_{ki} + 2D_{u_i u_j}. \tag{47c}$$

We henceforth consider the axisymmetric case ($\partial_y = 0$) for simplicity. As shown below, the left-hand sides of Eqs. (47b) and (47c) are typically negligible. Assuming for now that this is true, Eq. (47c) can be solved for the velocity dispersion,

$$\begin{pmatrix}\Pi_{xx}\\ \Pi_{xy}\\ \Pi_{yy}\end{pmatrix} = t_{\mathrm{stop}}\begin{pmatrix}1 & -2\tau_{\mathrm{s}} & 0\\ \tau_{\mathrm{s}}/4 & 1 & -\tau_{\mathrm{s}}\\ 0 & \tau_{\mathrm{s}}/2 & 1\end{pmatrix}^{-1}\begin{pmatrix}D_{u_x u_x}\\ D_{u_x u_y}\\ D_{u_y u_y}\end{pmatrix} = \frac{t_{\mathrm{stop}}}{1+\tau_{\mathrm{s}}^2}\begin{pmatrix}1+\tau_{\mathrm{s}}^2/2 & 2\tau_{\mathrm{s}} & 2\tau_{\mathrm{s}}^2\\ -\tau_{\mathrm{s}}/4 & 1 & \tau_{\mathrm{s}}\\ \tau_{\mathrm{s}}^2/8 & -\tau_{\mathrm{s}}/2 & 1+\tau_{\mathrm{s}}^2/2\end{pmatrix}\begin{pmatrix}D_{u_x u_x}\\ D_{u_x u_y}\\ D_{u_y u_y}\end{pmatrix}, \tag{48}$$

which recovers Eqs. (35a)–(35c) once we identify $\{\Pi_{xx}, \Pi_{xy}, \Pi_{yy}\} = \{\langle u_p^2\rangle, \langle u_p v_p\rangle, \langle v_p^2\rangle\}$ and apply Eq. (45).

Equation (47b) can be solved for the mean velocity

$$\begin{pmatrix} U_x \\ U_y \end{pmatrix} = -\frac{1}{\Sigma}\frac{t_{\rm stop}}{1+\tau_s^2}\begin{pmatrix} 1 & 2\tau_s \\ -\tau_s/2 & 1 \end{pmatrix}\partial_x \begin{pmatrix} \Sigma\Pi_{xx} \\ \Sigma\Pi_{xy} \end{pmatrix}. \tag{49}$$

We now assume that Σ varies on a shorter length scale than $t_{\rm stop}$ or Π_{ij} do. The diffusion equation, from Eq. (47), takes the simple form

$$\partial_t \Sigma = D_{{\rm p},x}\partial_x^2 \Sigma, \tag{50}$$

where

$$\begin{aligned} D_{{\rm p},x} &= \frac{t_{\rm stop}}{1+\tau_s^2}(\Pi_{xx} + 2\tau_s\Pi_{xy}) \\ &= \left(\frac{t_{\rm stop}}{1+\tau_s^2}\right)^2 \left(D_{u_x u_x} + 4\tau_s D_{u_x u_y} + 4\tau_s^2 D_{u_y u_y}\right) \end{aligned} \tag{51}$$

in exact agreement with Eq. (36).

We now determine the conditions under which the left-hand sides of Eqs. (47b), (47c) may be neglected. Let L be the length scale (in the x-direction) over which $\ln\Sigma$ varies, and let T be the timescale. Then U_i also varies on length- and timescales L and T (Eq. (49)), with amplitude $U_i \sim L/T$ (Eq. (47), and Π_{ij} is constant (Eq. (48)), with $\Pi_{ij} \sim C^2$, where C is the typical random speed. The left-hand side of Eq. (47b) is smaller than the first term on the right-hand side when $L/T \ll C$. As long as this inequality holds, the two terms on the right-hand side tend to equalize, with $C^2T/L^2 \sim A_{ij}$, and the terms on the left-hand side of Eq. (47c) (other than the Ξ_{kij} term) are smaller than the "$A\Pi$" terms on the right-hand side by $(L/CT)^2 \ll 1$; the Ξ_{kij} is smaller than the "$A\Pi$" terms by $L/CT \ll 1$. In sum, our approximations are valid as long as $L/T \ll C$, i.e., that the mean speed of the particles is less than their random speed. As long as this holds, the timescales for both the mean speed and the random speed to reach their quasi-steady-state values of Eqs. (48) and (49) are much shorter than the diffusion timescale T.

We return briefly to the discussion in Section 4.2.1 of whether particle concentration relative to gas is the fundamental quantity diffused by turbulence. Equation (49) shows that, for $\tau_s \ll 1$ (to ignore the complexities of orbital motions), $\Sigma\Pi_{xx}$ is the diffused quantity, which is not proportional to relative concentration. However this result is restricted to $t_{\rm stop} \gg t_{\rm eddy}$. The standard assumption that diffusion levels concentration gradients holds for small particles tightly coupled to eddies. Since this limit is not treated by the Fokker–Planck approach, there is no inconsistency.

6. Neglected effects

6.1. Collisions

Interparticle collisions are neglected both to simplify the analysis and because they are often a small correction to the dynamics, when compared to gas drag. The collision time is

$$t_{\rm coll} = \frac{2\rho_\bullet a}{3\rho_p v_{\rm rel}} \tag{52}$$

where $v_{\rm rel}$ is the relative velocity between particles and $\rho_\bullet \sim$ 1–3 g/cm^3 is the internal solid density. For collisions between two species i and j,[13] the collision time for species i due to j is set by the space density of j and particle radius, $a \to 2a_j^3/(a_i^2 + a_j^2)$.

If we compare to the stopping time in the Epstein regime, $t_{\rm stop}^{\rm Ep} = \rho_\bullet a/(\rho_g c_g)$, we see that

$$\frac{t_{\rm stop}^{\rm Ep}}{t_{\rm coll}} \simeq \frac{\rho_p}{\rho_g}\frac{v_{\rm rel}}{c_g} \ll 1, \tag{53}$$

where inequality follows since both fractions are less than unity in a smooth turbulent disk.[14] The particle density should be less than the gas density for our test particle approach (see Section 6.3) and the relative motions between particles (whether induced by turbulence or aerodynamic drift) are always subsonic.

In the Stokes regime (when the particle radius exceeds the gas mean free path, λ, but the Reynolds number of the flow around the particle remains below unity) collisions become relatively more important as the stopping time increases by $4a/(9\lambda) > 1$. However turbulent drag sets in before collisions dominate in gas rich disks. For turbulent drag, $t_{\rm stop}^{\rm turb} \approx \rho_\bullet a/(\rho_g \Delta V)$, where ΔV is the relative velocity of particles and gas. By this point (Appendix A) particles are sufficiently decoupled from the gas that $v_{\rm rel} \approx \Delta V$, and

$$\frac{t_{\rm stop}^{\rm turb}}{t_{\rm coll}} \approx \frac{\rho_p}{\rho_g} \tag{54}$$

gives the result (for turbulent drag) that drag is more significant than collisions if the local mass in gas exceeds that in particles. We showed above that this criterion is overrestrictive in the linear drag regimes (Stokes and Epstein).

6.2. Spatial spectrum of eddies and crossing trajectories

Unlike the detailed treatments pioneered by Völk et al. (1980), we neglect the spatial spectrum of turbulence. This is valid if the time to cross an eddy, $t_{\rm cross} = \ell_{\rm eddy}/\Delta V$ (with $\ell_{\rm eddy}$ the largest eddy scale and ΔV the relative motion of particles and gas), is small compared to either the eddy time (so that a particle never sees the spatial extent of an eddy) or the stopping time (so that a particle is fully accelerated before crossing an eddy). Thus spatial homogeneity is a good approximation for

$$t_{\rm cross} > \min(t_{\rm stop}, t_{\rm eddy}). \tag{55}$$

If ΔV arises from turbulent forcing, then this criterion is satisfied. For tight coupling, $St \ll 1$, tight coupling to eddies gives $\Delta V \ll \delta V_g$. Thus $t_{\rm cross}/t_{\rm eddy} = \delta V_g/\Delta V \gg 1$, and $t_{\rm cross}/t_{\rm stop}$ is even larger, so Eq. (55) is readily satisfied. For loose coupling,

[13] Our stirring model assume a single particle size. Since we work in the test particle limit with no particle collisions, our results can be applied to a dispersion of particle sizes with no additional approximation.

[14] If significant clumping to $\rho_p > \rho_g c_g/v_{\rm rel} \gg \rho_g$ occurs, from, e.g., streaming and/or gravitational instabilities, then collisions would become dynamically significant.

$St \gg 1$, the particle RMS motions are small so $\Delta V \sim \delta V_g$, the gas forcing. Thus $t_{cross}/t_{eddy} \sim \ell_{eddy}/(\delta V_g t_{eddy}) = 1$, and Eq. (55) is only marginally satisfied.

Orbital oscillations further help to confine particles to an eddy because the size of epicyclic or vertical oscillations, ℓ_{epi}, is smaller than the eddy scale:

$$\frac{\ell_{epi}}{\ell_{eddy}} = \frac{\delta V_p}{\Omega \ell_{eddy}} = \frac{\delta V_p}{\delta V_g} \sim \frac{1}{\sqrt{St}} \gg 1. \tag{56}$$

The above assumes $\tau_e \sim 1$ and $St \gg 1$ to that particle complete epicycles. We conclude that spatial homogeneity is a safe approximation for pure turbulent forcing, with (as usual) possible corrections near $\tau_s = 1$.

However if ΔV is dominated by net motion of particles relative to gas eddies, the spatial extent of the eddies can be significant. Cuzzi et al. (1993) follow Csanady (1963) in describing this as the "crossing trajectories effect" (hereafter CTE). Azimuthal and radial drift of particles due to radial pressure gradients, $\partial P/\partial r$, is the most likely source of net motion.[15] The radial and azimuthal drift speeds in the test particle limit are (Nakagawa et al., 1986):

$$\Delta V_r = -\frac{2\tau_s}{1+\tau_s^2}\eta v_K, \tag{57}$$

$$\Delta V_\phi = \frac{\tau_s^2}{1+\tau_s^2}\eta v_K, \tag{58}$$

where the dimensionless pressure support parameter,

$$\eta \equiv -\frac{\partial P/\partial \ln r}{2\rho_g v_K^2} \approx 1.5\left(\frac{c_g}{v_K}\right)^2, \tag{59}$$

and v_K is the Keplerian orbital speed.

For loose coupling, azimuthal drift at the full $\Delta V_\phi \approx \eta v_K$ dominates the net motion. Equation (55) will be satisfied (and the CTE will be ignorable) if turbulence is sufficiently strong so that $\delta V_g > \eta v_K$. If we model the turbulence as $\delta V_g \sim \sqrt{\alpha} c_g$, then $\alpha > \eta \sim 10^{-3}$ is required, i.e., reasonably, but not exceptionally strong turbulence. For tight coupling, radial drift dominates relative motion with $\Delta V_r \approx \eta v_K \tau_s \ll \eta v_K$. Equation (55) is satisfied for $\delta V_g > \eta v_K \tau_s^2$ or $\alpha > \eta \tau_s^4$. Thus even very weak turbulence ($\alpha \gtrsim 10^{-16}$ for mm-sized pebbles at 1 AU) will negate the CTE for $\tau_s \ll 1$.

When the CTE is relevant, our results should apply approximately for an effective eddy time, t'_{eddy}, that is the smaller of the actual eddy time and the crossing time,

$$t'_{eddy} \approx \left(1/t_{eddy}^2 + 1/t_{cross}^2\right)^{-1/2} \approx t_{eddy}/\sqrt{1+(\Delta V/\delta V_g)^2}. \tag{60}$$

This correction factor is similar to that used by Cuzzi et al. (1993) in their Eqs. (43) and (B.12).[16] Our prediction also appears consistent with Völk et al. (1980), in particular Fig. 1 of the related Völk et al. (1978) (where our relative drift ΔV is their V_L).

6.3. Particle feedback and concentration

We model the passive response of particles to imposed turbulence, ignoring the aerodynamic feedback of particles on turbulent gas dynamics. This restricts our analysis to local particle densities below the gas density, $\rho_p \ll \rho_g$. This approximation is roughly valid for turbulence strong enough and/or particles small enough to prevent settling to such high densities. Specifically, $\rho_p/\rho_g \simeq (\Sigma_p/\Sigma_g)(H_g/H_p) \lesssim 1$ requires

$$\alpha_z \gtrsim (\Sigma_p/\Sigma_g)^2 \tau_s \sim 10^{-4}\tau_s, \tag{61}$$

from Eq. (23), and a nominal $\Sigma_p/\Sigma_g \sim 10^{-2}$. Enhancements of solid column densities relative to gas requires even stronger turbulence to remain in the test particle limit. It is difficult to keep large particles from settling, but if only a small mass fraction resides in large particles, feedback effects might remain small.

Drag feedback effects are known to trigger turbulence by themselves. Shear-induced instabilities from particle settling, i.e., Kelvin–Helmholtz instabilities, have been identified as a foil to the gravitational collapse of solids (Weidenschilling, 1980; Cuzzi et al., 1993). Recently it has been shown that the in-plane drift of solids and gas triggers instabilities and turbulence when feedback is included (Youdin and Goodman, 2005; Youdin and Johansen, 2007). These "streaming" instabilities are particularly relevant since they generate significant particle clumping (Johansen and Youdin, 2007) even when shear is also included (Johansen et al., 2006a).

In addition to the streaming instability, other effects cause particles to concentrate in turbulent flows, as discussed in the introduction. Most concentration mechanisms are size dependent and transient. (Appendix B mentions the likely destruction long-lived vortices in 3-D.) Nevertheless non-diffusive behavior, especially on the integral scale of turbulence as seen in Johansen et al. (2006a), may cause discrepancies with our simplified turbulence model. In the absence of gravitational collapse diffusion should still occurs on long length and time scales. Comparing our results to simulations (and parameter regimes) with different degrees of particle concentration will deepen our understanding of non-diffusive and other intermittent turbulent behaviors. For instance treating the global pressure gradients (and hence radial drift) as a free parameter should modulate particle concentration. Drift that is either too strong (blasting through any eddy) or too slow (reducing the pileups in an eddy time) should reduce particle concentration.

7. Discussion

We study the diffusion of particles, and the excitation of their random velocities, by turbulent forcing in Keplerian gas disks. We obtain an improved result for radial particle diffusion in Eqs. (36) and (51) (identical formulae from independent techniques). We express radial particle diffusion in an approximate form for isotropic turbulence in Eq. (37) and even more crudely

[15] Vertical settling can be neglected as it is smaller than particle (and thus gas) RMS speeds from Eq. (27).

[16] Though Cuzzi et al. (1993) apply the correction for all St, even if $t_{stop} \ll t'_{eddy}$, and there should be no effect if the particles are fully accelerated before crossing an eddy.

(good for quick estimates) in Eq. (5),

$$Sc_x \equiv \frac{D_{g,x}}{D_{p,x}} = \frac{(1+\tau_s^2)^2}{1+4\tau_s^2} \sim 1+\tau_s^2. \quad (62)$$

Our result improves on the estimate of particle diffusion in Cuzzi et al. (1993), $Sc_{CDC} = 1 + St = 1 + \tau_s/\tau_e$, by including orbital dynamics and calculating diffusion for longer than a single eddy time (see Section 4.1.1). The discrepancy with the Cuzzi et al.'s (1993) value is only significant for large particles with stopping times longer than the eddy or orbital time.

Our new results for in-plane velocity dispersions, Eq. (33), combine turbulent forcing and epicyclic motions. Our results for vertical stirring in Section 4.2 agree with previous authors, including Cuzzi et al. (1993) (see their Eq. (53)) and Dubrulle et al. (1995) for tight particle coupling, and Carballido et al. (2006) for loose particle coupling. We add a correction for arbitrary eddy times which reduces particle velocities (Eq. (20)) and scale heights (Eq. (21)) for long eddy times. We include simple, physically motivated prescriptions to generalize the scale height result to include thorough mixing of small particles with gas (Eq. (28)) and to describe the reduction of the effective (Lagrangian) eddy time due to particle drift (Eq. (60)).

We do not imagine that our results will significantly influence collisional velocities since the RMS velocities we calculate have a similar scaling to previous results. Order unity corrections are possible for collisions involving marginally coupled particles, as orbital dynamics becomes important and the drift through eddies is maximized, but that calculation was beyond the scope of this work.

The rates of gravitational collapse of large particles, which are limited by mass diffusion when Toomre's $Q > 1$, will be increased. Preliminary investigations indicate that the rate of dissipative gravitational collapse remains constant as $\tau_s \to \infty$ while the Cuzzi et al.'s (1993) result would predict a growth rate that falls as τ_s^{-1} (Youdin, in preparation). Other instabilities limited by particle diffusion may be influenced as well.

The detailed predictions of random velocities should prove useful in the interpretation of numerical simulations which couple particle dynamics to (usually MHD) turbulence. Carballido et al. (2006) already confirmed their results for vertical oscillations with simulations of MRI driven turbulence. It remains to perform numerical tests of in-plane motions, but note that Carballido et al. (2006) have already recovered the expected epicyclic velocity dispersions (radial speeds twice azimuthal) for $\tau_s = 10$ particles. Ideally simulations of forced turbulence could investigate the effects of variable eddy times.

We can apply our results the chemical gradients in the Solar System. A notable example is the spectroscopic zonation of the asteroid belt, but the issue is more general (Taylor, 2001). We consider, very roughly, the minimum size a particle must have to drift radially faster than it diffuses, which is a crude measure of whether particles of a given size could maintain zonation over a drift time. Using the α-parameterization for turbulent gas diffusion, $D_{g,x} \equiv \alpha_x c_g^2/\Omega$, Eqs. (5) and (57) give the ratio of drift to diffusion time (over a scale of the disk radius r) as $t_{drift}/t_{diff} \sim \alpha_x/\tau_s$. Any particle with $\tau_s > \alpha_x$ will diffuse slower than it migrates radially, i.e., a particle bigger than a centimeter for $\alpha_x \approx 0.01$ at $r \sim 2.5$ AU. This simple result deserves two comments. First it is the same criterion for a particle to be large enough to sediment to the midplane, from Eq. (23) (as long as $\alpha_x \sim \alpha_z$ which holds at least to order-of-magnitude). Second, since $\alpha_x \ll 1$ for subsonic turbulence, this fiducial particle size is tightly coupled, and could have been obtained equally well from the Cuzzi et al.'s (1993) result. Thus even though Cuzzi et al. (1993) overpredict the diffusion of large particles, the global implications are minor: large particles drift aerodynamically faster than they diffuse (with either result).

The reduced diffusion of heavy particles would slow the loss of particles from pressure maxima (Whipple, 1972), including anti-cyclonic vortices, where radial drift is reduced. Our improved result for diffusion is most relevant on smaller length scales, where diffusion rates are faster. This is the case for the dissipative gravitational instabilities mentioned above.

Appendix A. Particle sizes and drag regimes

To translate from τ_s to particle radius, a, we consider spherical particles of internal density $\rho_\bullet = 2$ g/cm^3. We use a standard minimum mass nebula model (Weidenschilling, 1977; Hayashi, 1981), which has a gas mean free path (evaluated in the midplane) (Nakagawa et al., 1986),

$$\lambda = \frac{\mu}{\rho_g \sigma_{mol}} \approx 1.2 \text{ m } \Sigma_{150}^{-1} \left(\frac{r}{5 \text{ AU}}\right)^{2.75}, \quad (A.1)$$

where $\mu = 3.9 \times 10^{-24}$ g is the mean molecular weight, and $\sigma_{mol} = 2 \times 10^{-15}$ cm^2 is the molecular cross section (Chapman and Cowling, 1970). The gas surface density profile, $\Sigma_g \propto r^{-3/2}$ is normalized to $\Sigma_{150} \equiv \Sigma_g(5 \text{ AU})/(150 \text{ g/cm}^2)$ at $r = 5$ AU.

When $a < 9\lambda/4$, Epstein drag from molecular collisions applies (Adachi et al., 1976). Then the particle size for a given (midplane) τ_s is

$$a_{Ep}(\tau_s) = \frac{\tau_s \Sigma_g}{\sqrt{2\pi}\,\rho_\bullet} \approx 30 \text{ cm } \tau_s \Sigma_{150} \left(\frac{r}{5 \text{ AU}}\right)^{-1.5}. \quad (A.2)$$

For $a > 9\lambda/4$, particles enter the viscous Stokes drag regime and

$$a_{St}(\tau_s) = \sqrt{\frac{9\mu c_g t_{stop}}{4\rho_\bullet \sigma_{mol}}} = 90 \text{ cm } \sqrt{\tau_s} \left(\frac{r}{5 \text{ AU}}\right)^{5/8}, \quad (A.3)$$

independent of gas density and with c_g as the sound speed. For linear drag the particle size is given by the *smaller* of a_{Ep} or a_{St}.

Drag forces become non-linear when the Reynolds number, $Re = \Delta V a/(\lambda c_g)$, of the flow around the particle exceeds unity. We take the relative motion of particles and gas, $\Delta V \sim \eta v_K \sim c_g^2/v_K$, from the pressure supported gas rotation a small fraction of the Keplerian speed, $v_K = \Omega r$, see Eq. (59). We estimate the size and stopping time, from Eq. (A.3), of the transition to turbulent drag as:

$$a_{turb} \sim \lambda v_K/c_g \approx 25 \text{ m } \Sigma_{150}^{-1} \left(\frac{r}{5 \text{ AU}}\right)^{2.5}, \quad (A.4)$$

Table 2
Symbols

Symbol	Definition/use	Meaning
Ω	v_K/r	Keplerian orbital frequency
t_{stop}	Eqs. (A.2), (A.3)	Particle stopping time
t_{eddy}	Eq. (9)	Eddy turnover time
t_{sett}	Eq. (2)	Vertical settling time
τ_s	Ωt_{stop}	Dimensionless stopping time
τ_e	Ωt_{eddy}	Dimensionless eddy time
St	t_{stop}/t_{eddy}	Stokes number
$Sc_{(x)}$	D_g/D_p, Eq. (37)	Schmidt number (radial)
D_g, $D_{p,(x)}$	Eqs. (11a)–(11c), (36)	Diffusion coefficients: gas and particle (radial)
$\alpha_{(x,z)}$	$D_g\Omega/c_g^2$, Eq. (23)	Dimensionless diffusion coefficients
H_p, H_g	Eq. (21)	Particle, gas scale heights
δV_g, δu_g, δw_g	Table 1	RMS turbulent speeds: isotropic, radial, vertical
δV_p, δu_p, δw_p	Eq. (3), Fig. 3	RMS particle speeds: isotropic, radial, vertical
$\langle u_g^2\rangle$, $\langle v_g^2\rangle$, $\langle w_g^2\rangle$	Eqs. (10), (B.1)	Mean squared turbulent gas speeds: radial, azimuthal, vertical
$\langle u_p^2\rangle$, $\langle v_p^2\rangle$, $\langle w_p^2\rangle$	Eqs. (13), (33a)–(33c), (20)	Mean squared random particle speeds: radial, azimuthal, vertical
$\langle u_g v_g\rangle$, $\langle u_p v_p\rangle$	Eqs. (B.1), (33c)	Velocity correlations: gas, particle
c_g	Eqs. (A.3), (A.4)	Isothermal sound speed
r	Eq. (A.1)	Radial distance from star
x, y, z	Eqs. (29a)–(29d), (18)	Local radial, azimuthal, vertical coordinates
ρ_p, ρ_g	Eq. (61)	Particle, gas space density
a, $\rho_\bullet$	Eqs. (A.2), (A.3)	Particle radius, internal density
Σ, Σ_g	Eq. (46a)	Particle, gas surface density
η	Eq. (59)	Pressure support parameter
ΔV	Eqs. (57), (58)	Particle-gas relative velocity

$$\tau_{s,turb} \sim \sqrt{2\pi}\frac{4\rho_\bullet\lambda}{9\Sigma_g}\left(\frac{v_K}{c_g}\right)^2 \approx 700\,\Sigma_{150}^{-2}\left(\frac{r}{5\text{ AU}}\right)^{3.75}. \qquad \text{(A.5)}$$

Our assumption of a linear drag law applies up to large particle sizes in the outer disk, but only for $\tau_s \lesssim 1$ at $r \lesssim 1$ AU.

Appendix B. Turbulence model for arbitrary eddy time

To numerically evaluate our results for in-plane particle stirring (Section 4.3), we relate the radial, azimuthal and correlated turbulent velocities ($\langle u_g^2\rangle$, $\langle v_g^2\rangle$, and $\langle u_g v_g\rangle$) as a function of τ_e. The essential assumption is that velocities are isotropic, which we show is reasonable even for spatially sheared eddies with $\tau_e \gg 1$. The detailed value of $\langle u_g v_g\rangle$ has a weak effect on particle stirring (and even then only near $\tau_s = 1$), but is included for completeness. We also argue that particle trapping is weak when eddies survive for only a single turnover time, even when that turnover time is long.

We separately consider the limiting cases of large and small τ_e. For $\tau_e \ll 1$ we take the unsheared turbulence to be isotropic, $\langle u_g^2\rangle = \langle v_g^2\rangle$. The velocity correlations are weak, and generated by the linear shear of radial velocity into azimuthal (which builds up for t_{eddy}) as $\langle u_g v_g\rangle \sim (3/2)\tau_e\langle u_g^2\rangle$.

The $\tau_e \gg 1$ case is more constrained by the dynamics of background shear. We introduce ω' as the perturbed vorticity of the turbulence on the outer scale, which we compare to the background shear vorticity, $\omega_K = -3\Omega/2$. (The ratio $|\omega'/\omega_K|$ is comparable to the ratio of turbulent speed to sound speed when the radial outer scale of the turbulence is comparable to the scale height.) We consider $|\omega'/\omega_K| < 1$, because the efficiency of converting vorticity from the background shear into turbulence is likely to be less than 100%. (Note however that $|\omega'/\omega_K| > 1$ is allowed for the forced $\tau_e \ll 1$ turbulence above.)

To build a model for $|\omega'/\omega_K| < 1$, we are guided by the dynamics of two-dimensional vortices, which have the following well-known properties (Saffman, 1992; Chavanis, 2000): (1) vortices exist in regions where the perturbed vorticity $\omega' < 0$ is more negative than the background vorticity; (2) vortices are elongated in the azimuthal direction by a factor $\Delta y/\Delta x \sim |\omega_K/\omega'|$ relative to their radial extent; (3) the radial and azimuthal (with Kepler shear subtracted) fluid velocities are $u_g \sim |\omega'^2/\omega_K|y$ and $v_g \sim -|\omega'|x$. Thus at the vortex edge $\langle u_g^2\rangle^{1/2} \sim \langle v_g^2\rangle^{1/2} \sim |\omega'|\Delta x$ and the velocities have the same magnitude; (4) the time for fluid to circulate around a vortex is $\sim 1/|\omega'|$.

We now depart from our analogy with long-lived two dimensional vortices which are absolutely stable in the absence of viscosity and are clearly not turbulence—since energy dissipation and angular momentum transport are absent. In three dimensions, though, vortices decay (Barranco and Marcus, 2005; Shen et al., 2006). We hypothesize that three-dimensional turbulence is characterized by the properties (2) and (3) of vortices listed above; and that, based on property (4), vortices live for a time $\sim 1/|\omega'|$ before decaying. Thus we assume $t_{eddy} \approx 1/|\omega'|$ so the assumption $|\omega'/\omega_K| \ll 1$ is equivalent to $\tau_e \gg 1$.

To calculate the $\langle u_g v_g\rangle$ for $\tau_e \gg 1$ we use the established relation that the energy dissipation rate is $3\Omega/2$ times the angular momentum flux (Lynden-Bell and Pringle, 1974; Lithwick and Chiang, 2007). [See Youdin and Johansen (2007) for how particle feedback introduces pressure work to the energy balance.] Since the energy dissipation rate is $\sim\langle u_g^2 + v_g^2\rangle/t_{eddy}$ and the angular momentum flux is $\langle u_g v_g\rangle$, we have $\langle u_g v_g\rangle \sim 2\langle u_g^2 + v_g^2\rangle/(3\tau_e)$.

Combining the results for the large and small τ_e regimes gives

$$\langle u_g^2\rangle = \langle v_g^2\rangle = \frac{2+9\tau_e^2/4}{3\tau_e}\langle u_g v_g\rangle. \quad \text{(B.1)}$$

The numerical coefficients should not be taken literally, but are for concreteness. The $\langle u_g v_g\rangle$ correlations given by Eq. (B.1) are a reasonable upper limit. In any event $\langle u_g v_g\rangle$ has only a moderate effect on particle stirring and only near $\tau_s = 1$. We also note that with an α-parametrization, $\langle u_g v_g\rangle \equiv \alpha c_g^2$, the standard approximation $V_{\rm turb} = \sqrt{\langle u_g^2 + v_g^2\rangle} \approx \sqrt{\alpha} c_g$ applies for hydro-turbulence only if correlations are strong $\langle u_g v_g\rangle \approx \langle u_g^2 + v_g^2\rangle$, i.e., near $\tau_e = 1$ in Eq. (B.1). In MRI turbulence on the other hand, α includes a dominant contribution from Maxwell stresses, so $V_{\rm turb} \approx \sqrt{\alpha} c_g$ can hold with weaker correlations.

Long-lived two-dimensional vortices can concentrate particles (de la Fuente Marcos and Barge, 2001). However since we assume that eddies only survive for a single turnover time, particle concentration is weak, and our diffusive treatment should be a good approximation. Because the drift speed of a particle towards the center of a vortex is[17] $u_{\rm drift} \sim v_g \tau_s/(1+\tau_s^2)$, the time for particles to reach the center of a vortex is $\Delta x/u_{\rm drift} \sim (\Delta x/v_g)(1+\tau_s^2)/\tau_s \sim t_{\rm eddy}(1+\tau_s^2)/\tau_s$, i.e., it is always longer than $t_{\rm eddy}$. Vortices must survive for many circulation times for particle concentration to be important.

Klahr and Henning (1997) consider particle concentration by a "sideways" vortex, i.e., a vortex whose rotation axis is parallel to the midplane. Such a vortex concentrates particles in the particles' settling time if $|\omega| \lesssim \Omega$. Klahr and Henning (1997) show that sideways vortices appear in 2D simulations of convection, so the efficiency of this mechanism in 3D with radial drift deserves more study.

References

Adachi, I., Hayashi, C., Nakazawa, K., 1976. The gas drag effect on the elliptical motion of a solid body in the primordial solar nebula. Prog. Theor. Phys. 56, 1756–1771.

Balbus, S.A., Hawley, J.F., 1991. A powerful local shear instability in weakly magnetized disks. I. Linear analysis. II. Non-linear evolution. Astrophys. J. 376, 214–233.

Barranco, J.A., Marcus, P.S., 2005. Three-dimensional vortices in stratified protoplanetary disks. Astrophys. J. 623, 1157–1170.

Binney, J., Tremaine, S., 1987. Galactic Dynamics. Princeton Univ. Press.

Carballido, A., Stone, J.M., Pringle, J.E., 2005. Diffusion coefficient of a passive contaminant in a local MHD model of a turbulent accretion disc. Mon. Not. R. Astron. Soc. 358, 1055–1060.

Carballido, A., Fromang, S., Papaloizou, J., 2006. Mid-plane sedimentation of large solid bodies in turbulent protoplanetary discs. Mon. Not. R. Astron. Soc. 373, 1633–1640.

Chamberlain, J.W., Hunten, D.M., 1987. Theory of Planetary Atmospheres: An Introduction to Their Physics and Chemistry. International Geophysics Series, vol. 36. Academic Press, Orlando.

[17] We neglect the extra drift caused by cause drag with the mean shear of the disk. This is appropriate if $|\omega'/\Omega| > H/r$, because then the non-Keplerian velocities due to the vortex are larger than those due to the mean shear. If this inequality were violated, then particle would drift straight through vortices and concentration would be negligible.

Chandrasekhar, S., 1943. Stochastic problems in physics and astronomy. Rev. Mod. Phys. 15, 1–89.

Chapman, S., Cowling, T.G., 1970. The Mathematical Theory of Non-Uniform Gases: An Account of the Kinetic Theory of Viscosity, Thermal Conduction and Diffusion in Gases. Cambridge Univ. Press, Cambridge.

Chavanis, P.H., 2000. Trapping of dust by coherent vortices in the solar nebula. Astron. Astrophys. 356, 1089–1111.

Csanady, G.T., 1963. Turbulent diffusion of heavy particles in the atmosphere. J. Atmos. Sci. 20, 201–208.

Cuzzi, J.N., Dobrovolskis, A.R., Champney, J.M., 1993. Particle-gas dynamics in the midplane of a protoplanetary nebula. Icarus 106, 102–134 (CDC).

de la Fuente Marcos, C., Barge, P., 2001. The effect of long-lived vortical circulation on the dynamics of dust particles in the mid-plane of a protoplanetary disc. Mon. Not. R. Astron. Soc. 323, 601–614.

Dominik, C., Tielens, A.G.G.M., 1997. The physics of dust coagulation and the structure of dust aggregates in space. Astrophys. J. 480, 647–673.

Dubrulle, B., Morfill, G., Sterzik, M., 1995. The dust subdisk in the protoplanetary nebula. Icarus 114, 237–246.

Dubrulle, B., Marié, L., Normand, C., Richard, D., Hersant, F., Zahn, J.-P., 2005. An hydrodynamic shear instability in stratified disks. Astron. Astrophys. 429, 1–13.

Fan, L., Zhu, C., 1998. Principles of Gas–Solid Flows. Cambridge Univ. Press.

Fromang, S., Nelson, R.P., 2005. On the accumulation of solid bodies in global turbulent protoplanetary disc models. Mon. Not. R. Astron. Soc. 364, L81–L85.

Fromang, S., Papaloizou, J., 2006. Dust settling in local simulations of turbulent protoplanetary disks. Astron. Astrophys. 452, 751–762.

Gammie, C.F., 1996. Layered accretion in T Tauri disks. Astrophys. J. 457, 355–362.

Goldreich, P., Ward, W.R., 1973. The formation of planetesimals. Astrophys. J. 183, 1051–1062.

Hawley, J.F., Gammie, C.F., Balbus, S.A., 1995. Local three-dimensional magnetohydrodynamic simulations of accretion disks. Astrophys. J. 440, 742–763.

Hayashi, C., 1981. Structure of the solar nebula, growth and decay of magnetic fields and effects of magnetic and turbulent viscosities on the nebula. Prog. Theor. Phys. 70, 35–53.

Hinze, J.O., 1959. Turbulence. McGraw–Hill.

Hogan, R.C., Cuzzi, J.N., 2007. Cascade model for particle concentration and enstrophy in fully developed turbulence with mass-loading feedback. Phys. Rev. E 75 (5), 056305.

Hubbard, A., Blackman, E.G., 2006. Planetesimal growth in turbulent discs before the onset of gravitational instability. New Astron. 12, 246–263.

Johansen, A., Klahr, H., 2005. Dust diffusion in protoplanetary disks by magnetorotational turbulence. Astrophys. J. 634, 1353–1371.

Johansen, A., Youdin, A., 2007. Protoplanetary disk turbulence driven by the streaming instability: Non-linear saturation and particle concentration. Astrophys. J. 662, 627–641.

Johansen, A., Henning, T., Klahr, H., 2006a. Dust sedimentation and self-sustained Kelvin–Helmholtz turbulence in protoplanetary disk midplanes. Astrophys. J. 643, 1219–1232.

Johansen, A., Klahr, H., Henning, T., 2006b. Gravoturbulent formation of planetesimals. Astrophys. J. 636, 1121–1134.

Johansen, A., Klahr, H., Mee, A.J., 2006c. Turbulent diffusion in protoplanetary discs: The effect of an imposed magnetic field. Mon. Not. R. Astron. Soc. 370, L71–L75.

Klahr, H.H., Henning, T., 1997. Particle-trapping eddies in protoplanetary accretion disks. Icarus 128, 213–229.

Klahr, H.H., Henning, T., Kley, W., 1999. On the azimuthal structure of thermal convection in circumstellar disks. Astrophys. J. 514, 325–343.

Landau, L.D., Lifshitz, E.M., 1959. Fluid Mechanics: Course of Theoretical Physics. Pergamon, Oxford.

Lin, D.N.C., Papaloizou, J., 1980. On the structure and evolution of the primordial solar nebula. Mon. Not. R. Astron. Soc. 191, 37–48.

Lithwick, Y., 2007. Non-linear evolution of hydrodynamical shear flows in two dimensions. Astrophys. J., in press. astro-ph/0702046.

Lithwick, Y., Chiang, E., 2007. Collisional particle disks. Astrophys. J. 656, 524–533.

Lynden-Bell, D., Pringle, J.E., 1974. The evolution of viscous discs and the origin of the nebular variables. Mon. Not. R. Astron. Soc. 168, 603–637.

Markiewicz, W.J., Mizuno, H., Voelk, H.J., 1991. Turbulence induced relative velocity between two grains. Astron. Astrophys. 242, 286–289.

Mizuno, H., Markiewicz, W.J., Voelk, H.J., 1988. Grain growth in turbulent protoplanetary accretion disks. Astron. Astrophys. 195, 183–192.

Nakagawa, Y., Sekiya, M., Hayashi, C., 1986. Settling and growth of dust particles in a laminar phase of a low-mass solar nebula. Icarus 67, 375–390.

Ormel, C.W., Cuzzi, J.N., 2007. Closed-form expressions for particle relative velocities induced by turbulence. Astron. Astrophys. 466, 413–420.

Rincon, F., Ogilvie, G.I., Cossu, C., 2007. On self-sustaining processes in Rayleigh-stable rotating plane Couette flows and subcritical transition to turbulence in accretion disks. Astron. Astrophys. 463, 817–832.

Saffman, P., 1992. Vortex Dynamics. Cambridge Univ. Press, Cambridge.

Safronov, V.S., 1969. Evoliutsiia Doplanetnogo Oblaka. Nauka, Moscow.

Schräpler, R., Henning, T., 2004. Dust diffusion, sedimentation, and gravitational instabilities in protoplanetary disks. Astrophys. J. 614, 960–978.

Sekiya, M., 1998. Quasi-equilibrium density distributions of small dust aggregations in the solar nebula. Icarus 133, 298–309.

Semenov, D., Wiebe, D., Henning, T., 2004. Reduction of chemical networks. II. Analysis of the fractional ionization in protoplanetary discs. Astron. Astrophys. 417, 93–106.

Shen, Y., Stone, J.M., Gardiner, T.A., 2006. Three-dimensional compressible hydrodynamic simulations of vortices in disks. Astrophys. J. 653, 513–524.

Stevenson, D.J., 1990. Chemical heterogeneity and imperfect mixing in the solar nebula. Astrophys. J. 348, 730–737.

Taylor, S.R., 2001. Solar System Evolution: A New Perspective. Cambridge Univ. Press, Cambridge.

Tchen, C.M., 1947. Mean value and correlation problems connected with the motion of small particles in a turbulent field. Ph.D. thesis, Delft University, Netherlands.

Toomre, A., 1964. On the gravitational stability of a disk of stars. Astrophys. J. 139, 1217–1238.

Turner, N.J., Willacy, K., Bryden, G., Yorke, H.W., 2006. Turbulent mixing in the outer solar nebula. Astrophys. J. 639, 1218–1226.

Völk, H.J., Jones, F.C., Morfill, G., Roeser, S., 1978. Induced velocities of grains embedded in a turbulent gas. Moon Planets 19, 221–227.

Völk, H.J., Jones, F.C., Morfill, G.E., Roeser, S., 1980. Collisions between grains in a turbulent gas. Astron. Astrophys. 85, 316–325.

Ward, W.R., 1976. The formation of the Solar System. In: Avrett, E.H. (Ed.), Frontiers of Astrophysics, pp. 1–40.

Ward, W.R., 2000. On planetesimal formation: The role of collective particle behavior. In: Origin of the Earth and Moon, pp. 75–84..

Weidenschilling, S.J., 1977. The distribution of mass in the planetary system and solar nebula. Astrophys. Space Sci. 51, 153–158.

Weidenschilling, S.J., 1980. Dust to planetesimals—Settling and coagulation in the solar nebula. Icarus 44, 172–189.

Whipple, F.L., 1972. On certain aerodynamic processes for asteroids and comets. In: A. Elvius (Ed.), From Plasma to Planet, pp. 211–232.

Youdin, A.N., 2005a. Planetesimal formation without thresholds I. astro-ph/0508659.

Youdin, A.N., 2005b. Planetesimal formation without thresholds II. astro-ph/0508662.

Youdin, A.N., Goodman, J., 2005. Streaming instabilities in protoplanetary disks. Astrophys. J. 620, 459–469.

Youdin, A.N., Johansen, A., 2007. Protoplanetary disk turbulence driven by the streaming instability: Linear evolution and numerical methods. Astrophys. J. 662, 613–626.

Youdin, A.N., Shu, F.H., 2002. Planetesimal formation by gravitational instability. Astrophys. J. 580, 494–505.